JOURNAL OF PETROLOGY

*Journal of Petrology*, 2020, Vol. 61, No. 10: egaa097
doi: 10.1093/petrology/egaa097
Advance Access Publication Date: 27 October 2020
Original Article

OXFORD

# Magma Mushes of the Fogo Island Batholith: a Study of Magmatic Processes at Multiple Scales

**B. Graham, G. Dunning and A. M. Leitch***

Department of Earth Sciences, Memorial University, St John's, NL A1B 3X5, Canada

*Corresponding author. Telephone: 1(709) 864 3306. Fax: 1(709) 864 2589. E-mail: aleitch@mun.ca

Received 19 September 2018; Accepted 14 September 2020

## ABSTRACT

This field, petrographic, and geochemical study examines mingling of compositionally similar rocks at multiple scales. Evidence of complex magma interaction in a multi-component crystal mush reservoir is preserved within the Wild Unit, located along the NE shoreline of Fogo Island, Newfoundland and Labrador, Canada. The irregular contacts and lack of chilled margins between units, the back-intrusion of younger units by older units, the similar composition of units, and an overlap in U–Pb zircon ages suggest that all units interacted as viscous crystal mushes at similar temperatures in the shallow crust. Abundant rounded to ellipsoidal magmatic enclaves, of which there are at least three populations based on composition and crystallinity, appear to represent separate magmas that were entrained either as earlier mush material or crystal-poor intrusions that experienced break-up. Evidence of changes in liquid environment at deeper levels is preserved both in the field and at the mineral scale, where it is highlighted by abrupt compositional spikes in traverses across early forming plagioclase and pyroxene crystals. Heterogeneity in textures and composition of both major minerals (plagioclase and pyroxene) and an accessory mineral (zircon) point to processes such as crystal exchange and capture affecting tonalite crystal mushes, magmatic enclaves, and other intrusions in the study area earlier in their histories at deeper levels.

**Key words:** magma mushes; multiple intrusions; intermediate magmas; complex zoning; zircon

## INTRODUCTION

Batholiths, such as the one underlying Fogo Island in Newfoundland, are the near-surface result of complex, long-lived magmatic systems that extend through the crust. Edmonds *et al.* (2019) provided a synopsis, based on a range of disciplines, of some current models of the architecture of such systems. They described staging reservoirs at different depths, where magmas may evolve and interact before eruption, although the architecture of the reservoirs may vary with tectonic settings.

Plutons are assembled in incremental pulses (Petford *et al.*, 2000; de Saint Blanquat *et al.*, 2011; Miller *et al.*, 2011), often in a sheet-like geometry (Walker *et al.*, 2007; A. F. Glazner, personal communication, 2019), although particularly in granitoid systems pulses may be difficult to distinguish (Glazner *et al.*, 2004). Studies directed at understanding intrusion histories within plutons include field and petrological investigations where contacts and fabrics are well exposed (e.g. Walker *et al.*, 2007; Webber *et al.*, 2015) and investigations featuring mineral chemistry and zonations, which record replenishment, remobilization and venting events (e.g. Claiborne *et al.*, 2010; Barnes *et al.*, 2019).

Common themes in many of these and many other works (e.g. Bergantz *et al.*, 2015) are that magmatic systems are mostly crystal rich, with pockets of melt relatively small and ephemeral; and that rheological properties, which strongly influence magmatic interactions, change significantly as crystallinity increases (Weinberg *et al.*, 2001; Wiebe *et al.*, 2007; Burgisser & Bergantz, 2011). At crystallinities as low as 20–25%, plagioclase-rich melts tend to form interlocking crystal networks (Philpotts & Caroll, 1996), and when the proportion of crystals to melt approaches 50% a rheological 'lock-in' point is reached (Marsh, 1981), although this

rigid network can be 'unlocked' by reheating events, such as magmatic recharge (Marsh, 2002; Wiebe *et al.*, 2004).

Our study area is an ideal location to test and demonstrate key concepts of magmatic emplacement within a batholith. The lightly studied bimodal Fogo Island Batholith formed over a few million years in a transtensional tectonic setting. Wild Cove East, on the NE edge of the batholith, is underlain by a well-exposed sequence of intermediate rocks, which we interpret to represent the final stages of magmatic activity in the area. Through detailed field mapping we identified the principal rock units and magmatic structures, such as pipes and schlieren, and constructed the history and dynamics of emplacement. Petrographic investigations were used to study mineral textures and estimate emplacement crystallinities. On a smaller scale, electron probe micro-analyzer transects revealed the complex, pre-intrusion history of some pyroxene and plagioclase crystals. New U–Pb ages further constrain the emplacement timing of the batholith.

## GEOLOGICAL SETTING

Fogo Island, located off the northern coast of Newfoundland, Canada (Fig. 1), is underlain by the Silurian–Devonian Fogo Batholith, along with several volcano-sedimentary sequences (Kerr, 2013). The Fogo Batholith is composed of plutonic rocks ranging from gabbro–diorite to granite (Fig. 2). It is interpreted to represent an amalgamation of multiple plutonic bodies, as indicated by limited geochronological data including a 411 ± 13 Ma Rb–Sr isotopic age on the northern Seldom Granite (Sandeman & Malpas, 1995) and U–Pb zircon ages of 420 ± 2 Ma and 408 ± 2 Ma from, respectively, a monzogranite and a quartz diorite of the Wild–Sandy Cove Suite (Aydin, 1994). These ages correlate with other Late Silurian–Devonian granitic and bimodal plutons in central Newfoundland including the 412 Ma Long Island pluton, a 424 ± 2 Ma gabbro phase of the Mount Peyton Batholith, the 408 ± 2 Ma Loon Bay batholith, and 422 ± 2 Ma granitic to diabasic composite dykes that intrude the Llandoverian Botwood Group on the Port Albert Peninsula, to the NE of the Loon Bay batholith (Elliot *et al.*, 1991; McNicoll *et al.*, 2006; Fig. 1).

Fogo Island is underlain by gabbroic rocks in the south and granitic rocks in the north (Fig. 2). The two major units were defined by Baird (1958) as the Seldom Gabbro and Shoal Bay Granite. Both Baird (1958) and Currie (1997) acknowledged the presence of hybridized intermediate rocks located between the granite and gabbro units, although only Currie (1997) defined them as a separate mixed unit. The arrangement of gabbroic rocks overlain by granitic rock has led researchers to interpret the island as a section through a bimodal magma chamber where dense mafic magma once underlay buoyant felsic magma. The configuration of the Fogo Batholith is similar to the mafic–silicic layered

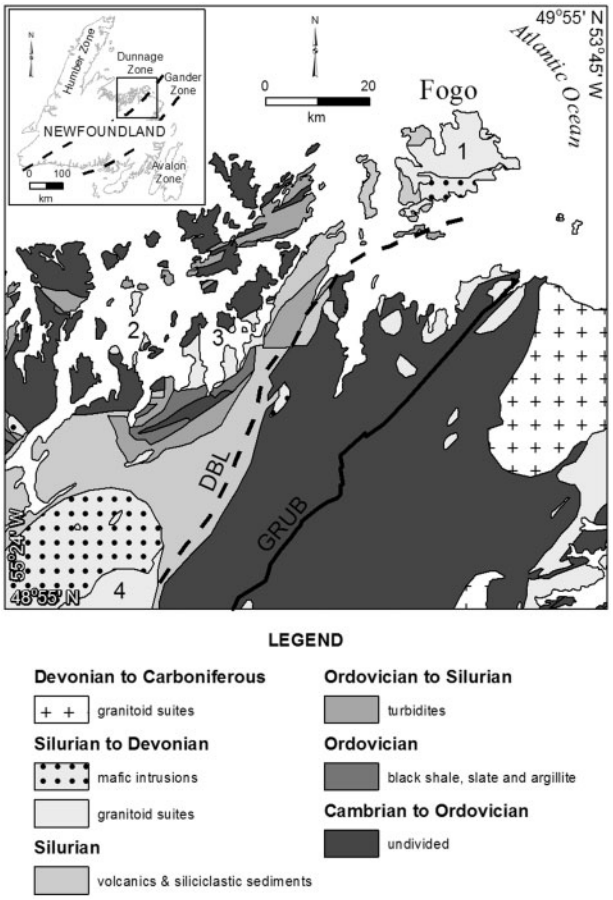


**Fig. 1.** Map of NE Newfoundland showing contemporaneous intrusions: 1, Fogo Island (408–420 Ma); 2, Long Island pluton (412 Ma); 3, Loon Bay intrusive suite (408 ± 2 Ma); 4, Mount Peyton Batholith (424 ± 2 Ma). The thick black line indicates the trace of the Gander River Ultramafic Belt (GRUB), a crustal-scale suture zone, separating the Gander and Dunnage tectonostratigraphic zones. The thick dashed line indicates the Dog Bay Line (DBL), along which there was strike-slip motion in the Silurian–Devonian. The dashed lines in the inset map delineate divisions in the deep crust determined by seismic surveys. (Map created by Neil Stapleton.)

intrusion (MASLI) model proposed by Wiebe (1996), where inputs of fresh mafic magma can have significant thermal and chemical influence on resident silicic magma.

Baird (1958) defined two volcaniclastic sequences on the NW part of the island. The Fogo Harbour Formation, composed of a mixture of sandstone and siltstone interlayered with felsic tuff units, is interpreted as the country rock into which plutons of the Fogo Batholith were intruded (Kerr, 2013). The Brimstone Head Formation is characterized by felsic volcaniclastic material and, based on a U–Pb zircon age of 421 ± 0·6 Ma from a basal rhyolite, may represent an extrusive component of the Fogo Island intrusion (Hamilton & Kerr, 2016).

A small ultramafic layered intrusion, called the Tilting Layered Suite (TLS), occurs in northeastern Fogo Island. Aydin (1994) identified two main crystallization sequences characterized respectively by early and late

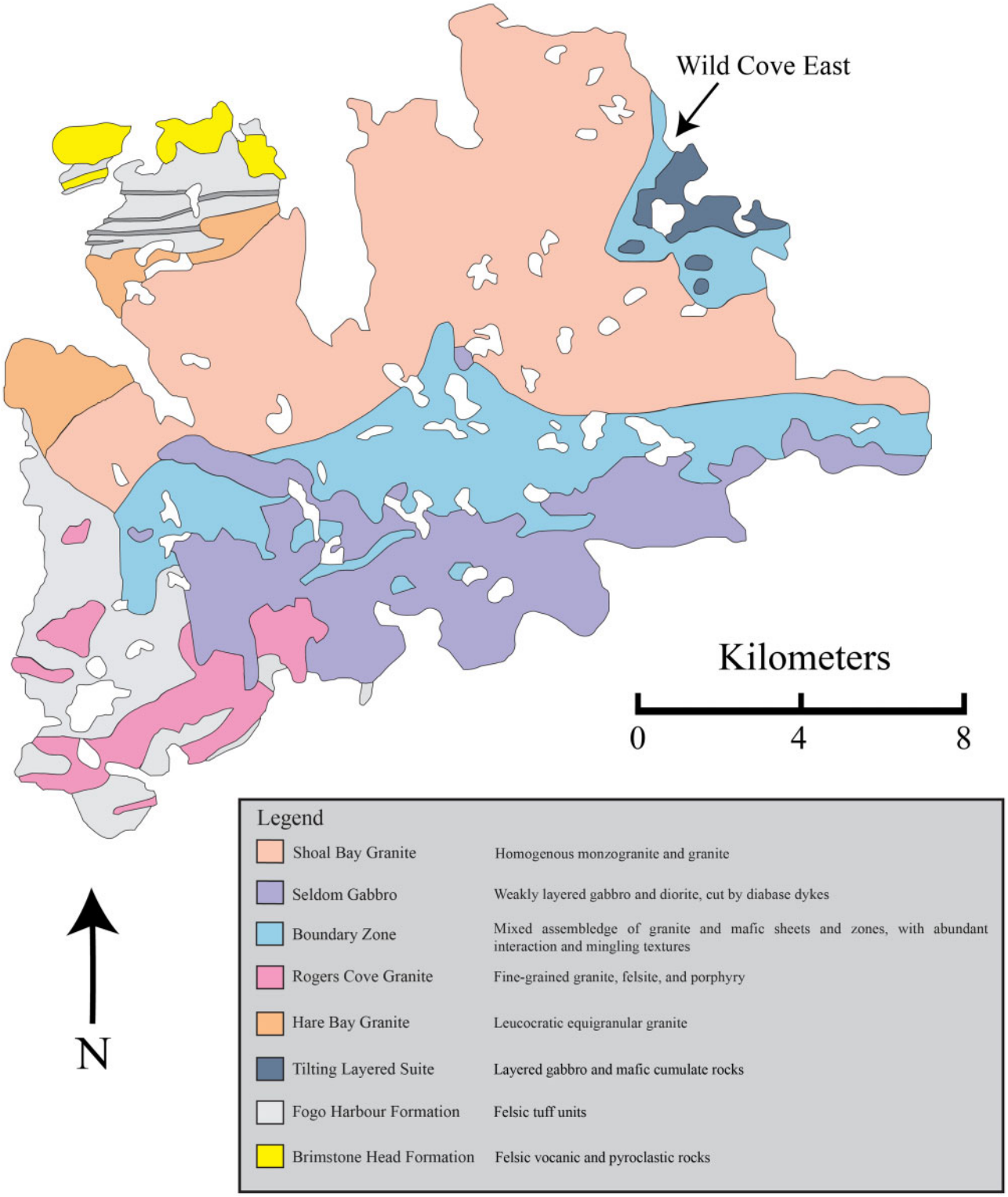


**Fig. 2.** Geological map of Fogo Island displaying major units and location of study area (Wild Unit). Modified after Baird (1958), Currie (2003) and Kerr (2013).

crystallization of cumulus orthopyroxene. It is unknown how the TLS relates to two surrounding high-level granitoid units: the Fogo Suite composed of monzogranite and minor granodiorite; and the Wild–Sandy Cove Suite (W–SCS) comprising diorite to tonalite. The Fogo Suite is generally free of inclusions whereas the W–SCS contains numerous country rock xenoliths and magmatic enclaves (Aydin, 1994). This study focuses exclusively on the Wild Unit, a subdivision of the W–SCS located at Wild Cove East (Fig. 2).

## FIELD EVIDENCE FOR MUSHES

### Methods

Because existing air photographs had inadequate resolution, remote imaging specialists CloudBreaker™ were hired to produce base maps of the field area. Using a drone helicopter, 735 high-resolution ortho-rectified images were taken at 50 m altitude over the entire field area, and at 25 m altitude over a specific area of interest. Cloudbreaker™ personnel stitched together the images into photo-mosaic base maps, which are available in Supplementary Data Electronic Appendix 1 (supplementary data are available at http://www.petrology.oxfordjournals.org). The base maps were printed out in two 2 m long sections; however, even at this high resolution, it was difficult to distinguish unit contacts amid fractures and surface staining. For accurate mapping, the first author traversed the area on foot, marking units and contacts on the base map, making detailed field observations and taking rock samples for further analysis.

### Map units and relationships

Three major host rock units are defined in the geological map in Fig. 3. Immediately inland, all exposed rocks are biotite granite, and we infer that this unit originally overlay the rocks in the study area, although it is a relatively minor component there now. Most rocks in the study area are intermediate and are divided into two groups based on the abundance of magmatic enclaves: for 'enclave-rich tonalites' they represent 5–20 % of the surface area whereas they are absent to scarce in 'enclave-poor tonalites'. Although tonalite is the field name used for both intermediate units, they span a modal compositional range from quartz diorite to tonalite. Modes were determined by point counting within multiple thin sections. In the field study, these slight variations in rock type could not be differentiated. The boundaries between all three units lack chilled margins. Miarolitic cavities, defined by 2–5 cm wide pockets of coarse-grained potassium feldspar and quartz, occur in both tonalite units. Fine-grained angular sedimentary xenoliths are common in the biotite granite unit.

### Interaction of mushes

#### *Intrusions*

A variety of dyke- or sill-like structures, ranging in both size and composition, are observed throughout the study area. Aydin (1994) defined three categories of intrusions in the Wild Unit: cross-cutting dykes displaying intact, continuous, and sharp margins; transitional dykes that display irregular and sigmoidal margins; and synplutonic dykes that are discontinuous, fragmented, and display host rock back-veining.

In general, cross-cutting dykes are the most compositionally distinct from their hosts and are interpreted to represent late felsic intrusions through crystalline rock that was below solidus temperatures. These late felsic dykes are found in all parts of the study area and generally strike to the north and dip steeply to the east.

Transitional dykes that display compositional similarity to their hosts are interpreted to represent earlier intrusions into a less rigid mush that was above solidus temperatures. These dykes occasionally contain magmatic enclaves. A pair of transitional quartz diorite dykes in the northernmost end of the study area (Fig. 4; location A in Fig. 3) display localized evidence for break-up into rounded globules owing to interaction with host tonalite mush material, and illustrate a potential magmatic enclave forming mechanism (Frost & Mahood, 1987). A diorite sill, 30 m wide in the horizontal where it is exposed along the coast and vertically at least 2 m thick (location B in Fig. 3), displays magmatic pipe structures that are not observed elsewhere in the field area. The sill shares irregular margins with the surrounding enclave-poor tonalite unit.

Clear evidence of intrusion into a mobile crystal mush is provided by the displacement of a 20 cm wide pyroxene-rich (~5 %) synplutonic tonalite dyke that cuts across both the enclave-poor tonalite and biotite granite units (Fig. 5; location D in Fig. 3). Despite being broken up, the original path of the intrusion can be easily inferred: pieces of the dyke are darker (owing to a higher abundance of clinopyroxene), finer-grained, and more angular than nearby magmatic enclaves (Fig. 6a). The degree of dyke displacement is noticeably higher in the enclave-poor tonalite unit compared with the biotite granite, indicating that the biotite granite was more cohesive at the time of intrusion, although it was not completely solid. In particular, where it crosses the biotite granite, fine cracks within the broken-up dyke segments are back-filled with felsic, phenocryst-free components of the host. The complexity of the mush movement is illustrated in Fig. 6b, where the dyke itself appears to have been intruded by enclave-rich tonalite.

Bordering the eastern end of the study area is an ~300 m wide mafic layered sill (location C in Fig. 3) that grades from enstatite hornblende troctolite at the bottom to biotite hornblende quartz diorite at the top and shares an irregular boundary with the adjacent enclave-poor tonalite unit. This represents the most mafic unit in Wild Cove East.

#### *Unit boundaries*

The boundaries between all units in the study area are consistently irregular and lack chilled margins, indicating the units coexisted at similar temperatures between the liquidus and solidus. The contact between the enclave-rich tonalite and enclave-poor tonalite is clearly visible in many parts of the field area but must be inferred in some areas based on the change in magmatic enclave abundance. In Fig. 7, magmatic enclaves terminate against a steeply dipping boundary and are noticeably more abundant on one side. Defining this boundary is a 5–10 cm thick anastomosing dark contact that is primarily

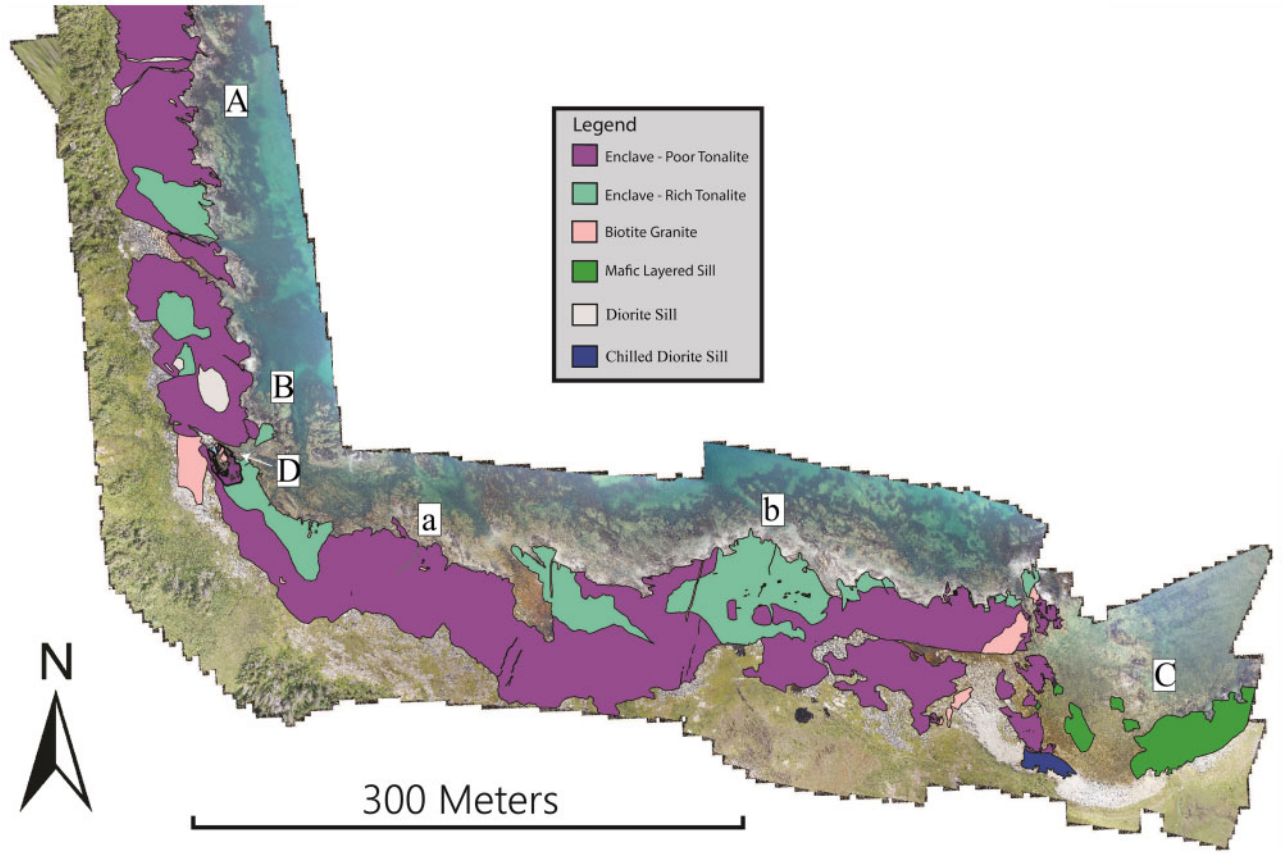


**Fig. 3.** Geological map of the Wild Unit produced in ArcMap. Digital base map provided by Cloudbreaker™ drone imagery. Locations of three prominent intrusions represented by A (quartz diorite dyke, Fig. 5), B (30 m wide diorite sill), C (mafic layered sill), D (detailed map area, Fig. 3). The chilled diorite sill is SW of the mafic layered sill. The location with the highest abundance of metasedimentary xenoliths is represented by (a) and the location with the largest enclaves is represented by (b) at UTM zone 21 N, 709980 m E, 5511555 m N.

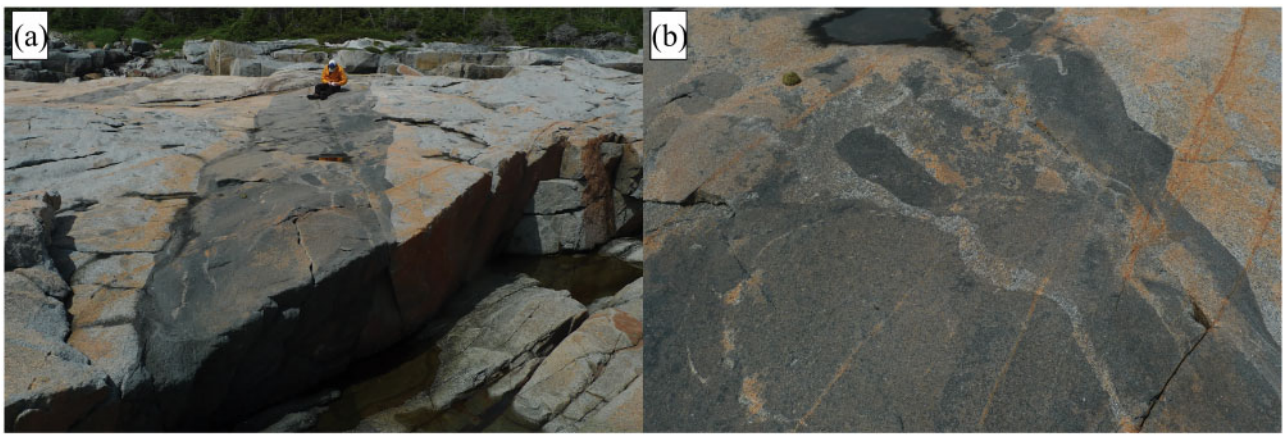


**Fig. 4.** Field photographs of quartz diorite dyke (location A in Fig. 3) that displays evidence of low rheological contrast between intruding and host magmas. (a) Dark 2 m wide biotite tonalite dyke intruding biotite hornblende tonalite host on the western side of the field area. The irregular boundary between dyke and host suggests that the two units mingled as crystal mushes as the time of intrusion. (b) Evidence of localized breakup of biotite tonalite dyke in rounded globules,.

composed of hydrothermally altered clinopyroxene, hornblende, and biotite (Fig. 7a). A smooth margin is seen on the enclave-poor tonalite side whereas a more irregular or cuspate boundary is seen on the enclave-rich tonalite side, suggesting a strong rheological gradient across these units (Fig. 7b).

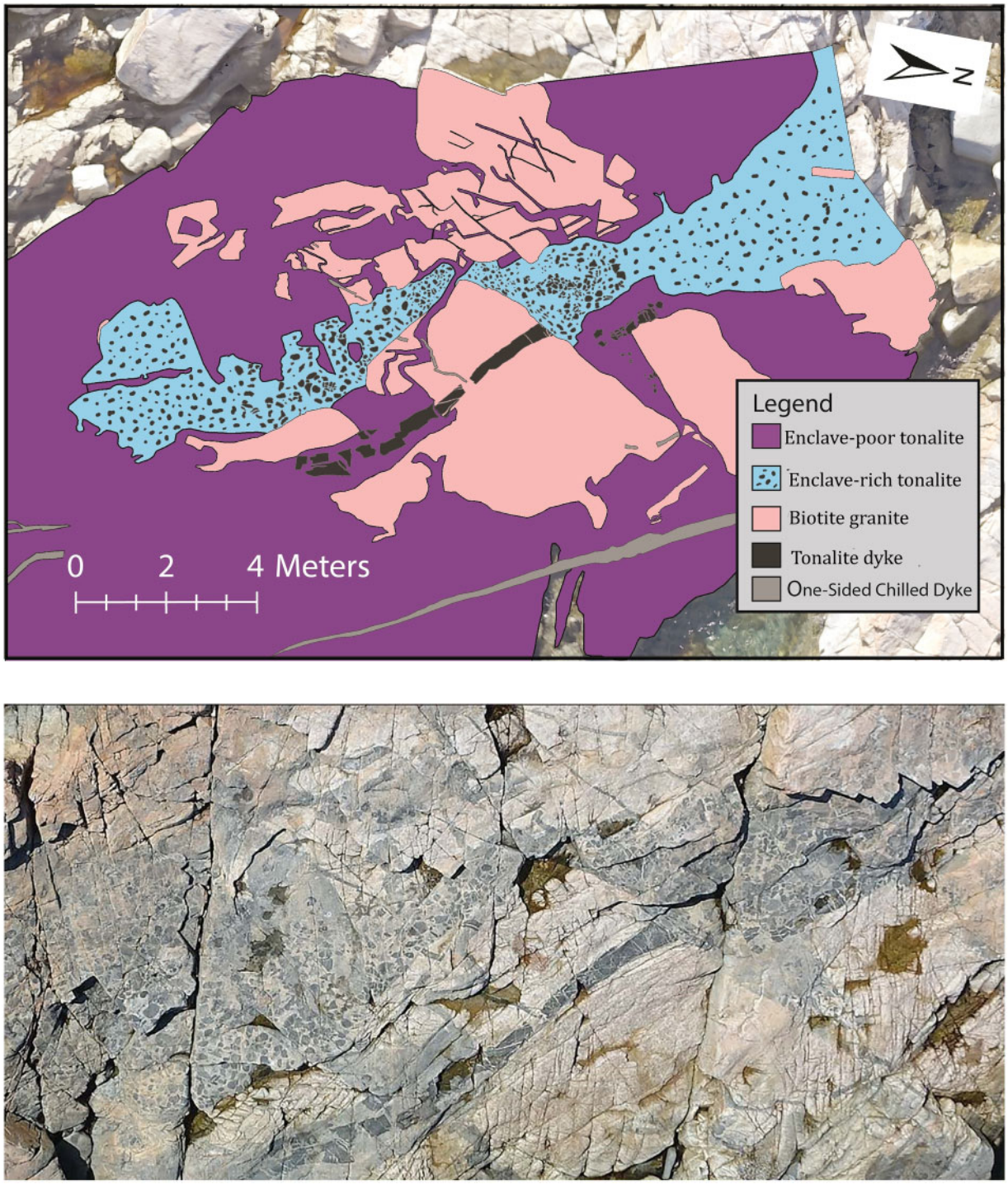


**Fig. 5.** Top: geological map of detailed map area, produced in ArcMap. Granite (pink) represents the oldest unit in map as it is intruded by both enclave-poor tonalite (purple) and enclave-rich tonalite (blue) units, the latter representing the youngest unit in unit in this map. A broken-up synplutonic dyke (black) is terminated against enclave-rich tonalite unit and intrudes both the enclave-poor tonalite and granite. Bottom: drone image of central region of the above map area.

The biotite granite shown in Fig. 5 is fully enclosed in both tonalite units, commonly shares an irregular boundary with each, and has a shallow-dipping contact (318/21 NE) with the overlying enclave-poor tonalite unit. The blocky shape of the unit suggests that it was rigid and brittle when the intermediate units intruded.

### *Magmatic enclaves*

Abundant rounded to ellipsoidal magmatic enclaves, which are finer-grained and darker than their hosts, represent the most striking evidence of magma mingling in the study area. Both the magmatic enclaves and the rocks that enclose them are medium to fine

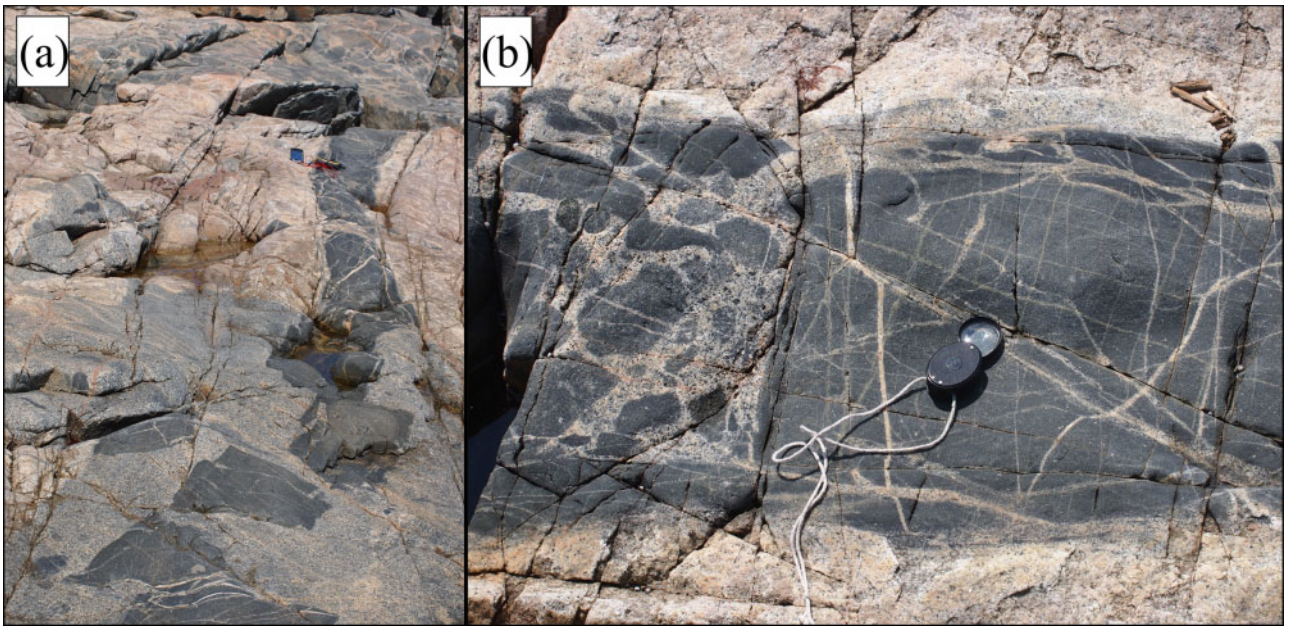


**Fig. 6.** Field photographs of broken-up tonalite dyke in the detailed mapping area (black unit in Fig. 5) that shows evidence of a relatively high rheological contrast between injecting and host magmas. (a) Looking NW at an angle along the surface, from near the SE extent of the dyke. The tonalite dyke is pulled apart in the grey enclave-poor tonalite unit (foreground) whereas it is relatively coherent in the pink biotite granite unit. Compass on the pink granite for scale. (b) A close-up, looking straight down, of the same dyke, where it is shown as discontinuous within biotite granite in Fig. 5. On the right, liquid from the biotite granite mush has back-intruded the broken-up tonalite dyke. On the left, enclave-rich tonalite appears to have displaced a section of the dyke.

grained and are ubiquitously intermediate in composition.

In many parts of the study area, particularly in the central and eastern regions of the enclave-rich tonalite, magmatic enclaves of differing mineralogy are observed close to and, in some cases, impinged against each other. In the centre of the detailed map area (Fig. 5, location D in Fig. 3), a high concentration of enclaves display vertical elongation and cluster in groups in rotational patterns. The largest magmatic enclaves are found on the eastern end of the enclave-rich tonalite, where they are elongated in an approximately east–west direction (average strike = 263) (location b in Fig. 3). Several have lengths exceeding 3 m.

### *Pipes and tubes or ladder structures*

Magmatic pipes, defined as steeply plunging cylindrical-shaped leucocratic structures that are mineralogically distinct from surrounding rock (Wiebe & Collins, 1998; Paterson, 2009), occur within the diorite sill (location B in Fig. 3). Examples of these structures were observed both in cross-sectional view and as rounded leucocratic 'tops' on the surface of the sill (Fig. 8a).

Immediately outside the sill margin, tube-like structures are present in the host tonalite. Like pipes, magmatic tubes form by the buoyant rise of magma through overlying denser material (Fig. 8b). These features tend to be of similar composition to the host material, and are generally distinguished only by a trail of rounded schlieren interpreted to represent lateral migration of the tube (Paterson, 2009). Because of limited vertical relief of the outcrop, the plunge of the tube structures could not be measured. Thus, it is unknown whether they best fit the steeply plunging 'tube' model of Paterson (2009), or the shallow-plunging 'ladder dyke' model of Glazner *et al.* (2012).

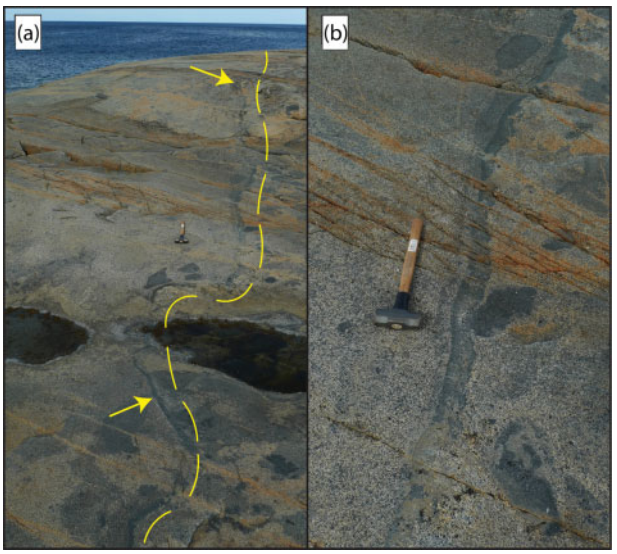


**Fig. 7.** Field photographs of visible contact between the enclave-poor tonalite and enclave-rich tonalite. (a) Dipping irregular contact between enclave-rich tonalite (right) and enclave-poor tonalite. Contact is located left of the dashed line. (b) At the boundary, clinopyroxene crystals have accumulated as a layer. This layer has a sharp contact against the enclave-poor tonalite (left), whereas the other contact is cuspate. A mafic magmatic enclave is seen impinging on the cuspate edge.

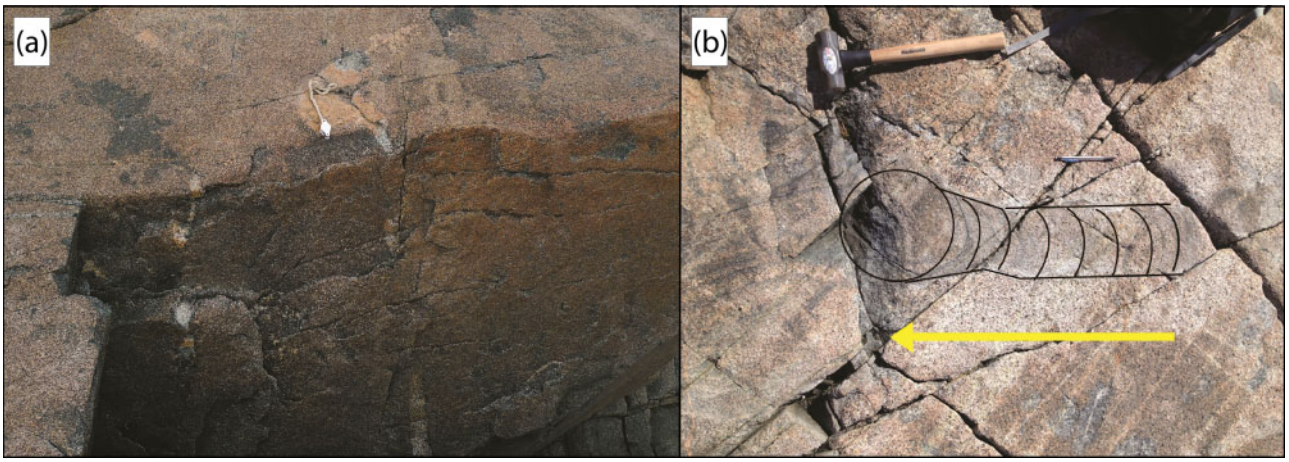


**Fig. 8.** Structures suggestive of compaction or filter pressing processes that can occur in crystal mushes observed in the diorite sill (location B in Fig. 3). (a) Magmatic pipe formed by buoyant rise of leucocratic magma through a more melanocratic host; defines vertical way-up direction in this part of study area (hand lens for scale). (b) Migrating magmatic tube structure (map view) defined by the buoyant rise of a magma through a mineralogically similar host. Arrow indicates lateral migration direction.

### *Schlieren*

Schlieren are defined as thin bands or layers of mafic material (typically biotite ± pyroxene) in granitoid bodies (Gilbert, 1906). Their origins are a subject of debate. Gently dipping schlieren have been attributed to current deposition and erosion in crystal-rich magmas (Gilbert, 1906; Emeleus, 1963) whereas the origin of steeply dipping schlieren has been linked to shear segregation in a crystal mush (Barriere, 1981; Abbott, 1989), crystal filtering (Weinberg *et al.*, 2001) and gravitational sinking of enclaves or xenoliths (Wiebe *et al.*, 2007). Rather than originating by these physical processes, they may be created by chemical processes such as diffusion and crystal ripening (Vernon and Paterson, 2006; Glazner, 2014).

Different styles of schlieren are observed in the two tonalite units of the Wild Unit. Schlieren in the enclave-poor tonalite consist of thin layers of biotite and hornblende in straight, steeply dipping planar sets up to 1 m wide and oriented approximately north–south ([176/80 W] and [172/80 W]). Shallow-dipping structures appear in localized parts of the unit. In the enclave-rich tonalite, schlieren are curved and commonly associated with the magmatic enclaves. In several cases, schlieren are found 'tailing behind' individual magmatic enclaves. In one case, the chilled outer margin of a magmatic enclave appears to be 'peeled off'.

## MINERAL TEXTURES AND MAGMATIC PROCESSES

### Methods

A total of 85 thin sections were examined for mineral abundances and textures. Most samples were gathered using a hammer and chisel; a portable diamond drill was used to obtain 2 inch core samples at key locations along flat outcrop. Samples were taken at scattered locations within the main units where minimal surface weathering was observed. Sample locations are provided in Supplementary Data Electronic Appendix 2, and petrographic features of the main units are summarized in Table 1.

In representative thin sections of the key units, estimates were made of the amounts of (1) euhedral plagioclase and pyroxene and large rounded resorbed phenocrysts; and (2) cores of euhedral crystals that showed resorption features. Photomicrographs across the entirety of a thin section were stitched together using Adobe Photoshop. The appropriate crystals were then outlined and the per cent area they represent was determined. As discussed below, we argue that these measures provide estimates of the emplacement crystallinity of some units. Results are summarized in Table 1.

### Textures in crystal mushes

The enclave-poor tonalite unit (Table 1) generally has less quartz, more clinopyroxene and a considerably higher proportion of subhedral crystals than the enclave-rich tonalite unit. Groundmass plagioclase grains are subhedral elongate to tabular (50–100 μm) whereas phenocrysts are tabular and subhedral (500–1000 μm). Quartz occurs as late interstitial grains or as medium-grained rounded amoeboid crystals. Many plagioclase grains, including groundmass and phenocrysts, display complicated zoning and resorption patterns and there is variability in the amount of resorption between thin sections taken from different parts of the unit. Plagioclase phenocrysts, which typically contain abundant inclusions of acicular apatite, are also the most common crystals to display internal mottling. Some quartz displays undulatory extinction presumably caused by stress after crystallization. Some clinopyroxene grains are corroded and mantled by hornblende and/or biotite whereas others are unaltered. They

**Table 1:** Petrographic features of key units at Wild Cove East

| | Sample unit | | | | | |
|---|---|---|---|---|---|---|
| | Biotite granite | Enclave-poor tonalite | Enclave-rich tonalite | Group 1 magmatic enclaves | Group 2 magmatic enclaves | Group 3 magmatic enclaves |
| Dominant minerals (%) | Qtz (40)<br>Kfs (35)<br>Pl (25)<br>Bt (<5) | Pl (75)<br>Qtz (10)<br>Cpx (10)<br>Bt (5)<br>Hbl (<5) | Pl (75)<br>Qtz (20)<br>Bt (5)<br>Cpx (<5)<br>Hbl (<5) | Pl (50)<br>Qtz (20)<br>Hbl (10)<br>Bt (10)<br>Cpx (5)<br>Opx (<5) | Pl (45)<br>Qtz (15)<br>Hbl (20)<br>Bt (10)<br>Cpx (5)<br>Opx (<5) | Pl (55)<br>Qtz (10)<br>Hbl (10)<br>Cpx (10)<br>Bt (5)<br>Opx (<5) |
| Accessory minerals | Fl, Py, Zrn | Ap, Ilm, Mag, Rt, Ttn, Zrn | Ap, Ilm, Mag, Rt, Ttn, Zrn | Ap, Ilm, Mag, Rt, Ttn, Zrn | Ap, Ilm, Mag, Rt, Ttn, Zrn | Ap, Ilm, Mag, Rt, Ttn, Zrn |
| Grain size | Medium | Medium | Medium | Fine | Fine | Medium |
| Estimated crystallinity (%) | n.a. | 50 (xtals)<br>20 (cores) | 20 | 15 | 30 | 35 |
| Field description | | | | Darker*, rounded, cuspate margins common, Pl phenocrysts | Darker*, rounded and commonly elongated, Pl phenocrysts | Similar colour index*, rounded and rarely elongated |

Mineral abbreviations (Kretz, 1983): Ap, apatite; Bt, biotite; Cpx, clinopyroxene; Fl, fluorite; Hbl, hornblende; Ilm, ilmenite; Kfs, potassium feldspar; Mag, magnetite; Opx, orthopyroxene; Pl, plagioclase; Py, pyrite; Qtz, quartz; Rt, rutile; Ttn, titanite; Zrn, zircon. n.a., not analyzed. See text for derivation of modes and crystallinity estimates.
*Colour compared with host.

generally occur as anhedral stubby or rounded crystals, often in clusters.

In the enclave-rich tonalite, plagioclase occurs as fine- to medium-grained (50–1000 μm) crystals that, in comparison with the enclave-poor tonalite unit, are rounded and lack well-defined crystal faces. Patchy zoning and mottled cores are common, with some displaying multiple stages of resorption–overgrowth whereas others show none, and minor clinopyroxene and apatite inclusions occur in some crystals. The textures and relative abundances of mafic minerals observed in the enclave-rich tonalite are similar to those seen in the enclave-poor tonalite. Biotite, pyroxene, and hornblende generally occur together in clusters at low abundances with biotite being the most abundant.

In the biotite granite, quartz generally occurs in coarse-grained clusters and is commonly embayed along shared boundaries with potassium-feldspar and other quartz. Plagioclase and potassium feldspar are commonly rounded and lack euhedral faces.

## Textures in magmatic enclaves

Magmatic enclaves are darker than their hosts, rounded or ellipsoidal in shape and have unchilled, sometimes cuspate boundaries. Based on field observations and petrography, samples were divided into three groups, with features summarized in Table 1. Group 1 enclaves are fine-grained, considerably darker than their hosts, contain feldspar phenocrysts, and typically have cuspate margins. Group 2 comprises dark fine-grained feldspar-phyric enclaves that are rounded and commonly elongated parallel to the primary magmatic fabric in the host tonalite mush. Group 3 magmatic enclaves are medium-grained, rounded and rarely elongated, and have a similar colour index to their hosts. Plagioclase phenocrysts in all enclave groups display mottled internal zones and/or embayed margins.

Group 1 magmatic enclaves are characterized by a fine-grained anhedral groundmass (100–250 μm diameter) composed primarily of plagioclase and quartz along with medium-grained rounded plagioclase phenocrysts (~1000 μm diameter). Normal and reverse zoning occurs in both the groundmass plagioclase grains and phenocrysts. Mafic minerals are hornblende and biotite and lesser amounts of clinopyroxene and orthopyroxene. Pyroxene is commonly found as corroded cores in hornblende and biotite. Compared with other magmatic enclave groups, there are low amounts of apatite and Fe–Ti oxide inclusions. Group 1 enclaves have the highest silica content (~60 wt%) and are classified as biotite hornblende tonalite.

Group 2 magmatic enclaves are the most common type in the study area. They are characterized by a high abundance of euhedral elongate plagioclase, and compared with Group 1 have lower amounts of quartz (15 % vs 20 %), higher amounts of hornblende (20 % vs 10 %), and larger amounts of apatite or Fe–Ti oxide inclusions. Plagioclase occurs as both fine-grained elongate laths in groundmass (25–100 μm) and as tabular phenocrysts (200–500 μm). Groundmass plagioclase laths generally display a preferred alignment. Where not mantled by hornblende or biotite, clinopyroxene occurs as small round crystals. Group 2 enclaves have intermediate silica content (~57 wt% $SiO_2$) and are classified as biotite hornblende tonalite.

The most distinct of the magmatic enclave groups is Group 3, which is characterized by a preferred alignment of particularly abundant and euhedral

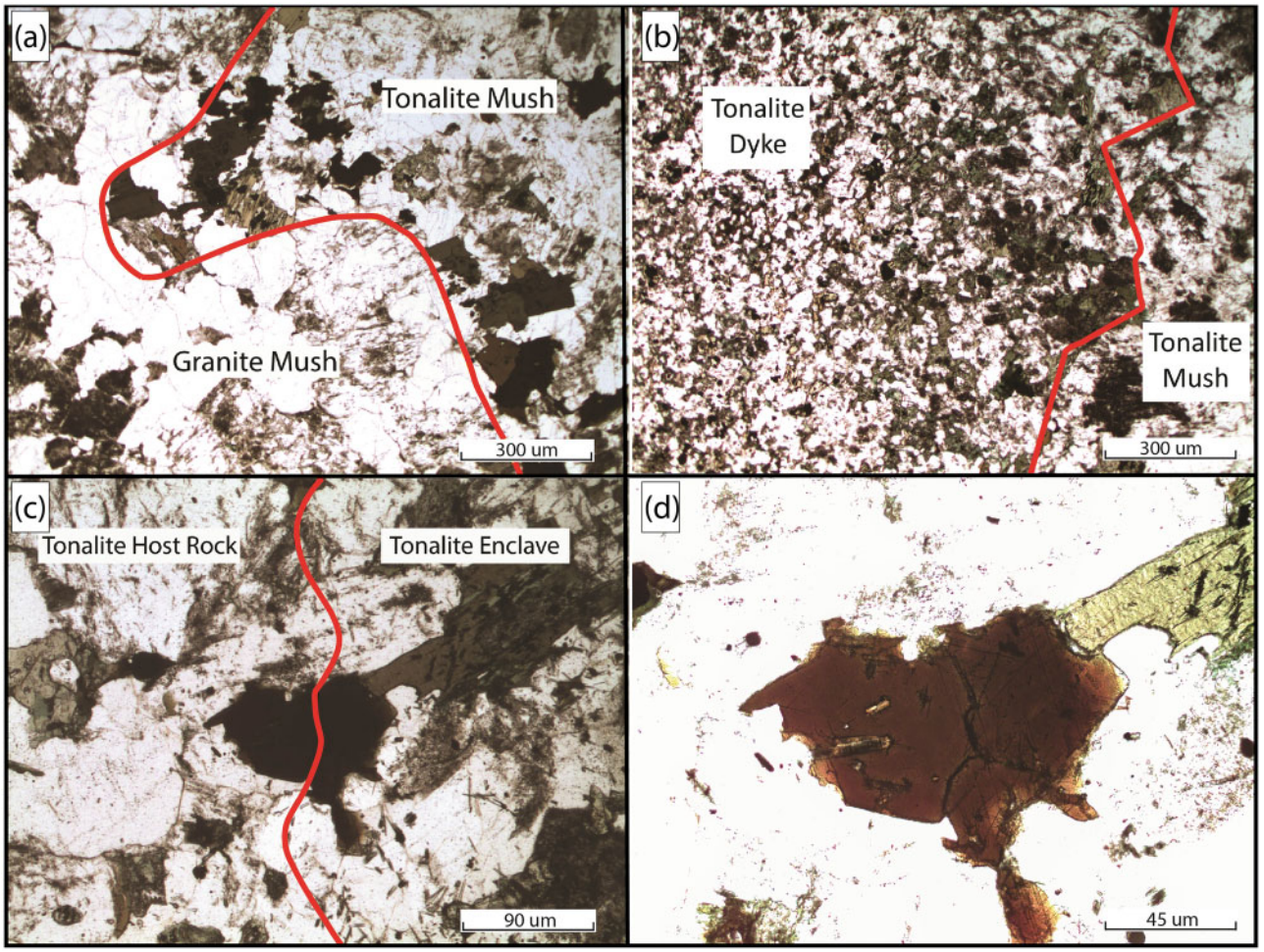


**Fig. 9.** Photomicrographs of contacts between units. (a) Irregular unchilled boundary between granite mush and enclave-rich tonalite mush. (b) Contact between disaggregated tonalite dyke and enclave-poor tonalite; abundance of hydrous minerals in tonalite dyke increases closer to the boundary with the tonalite mush. (c) Biotite along interpreted boundary between tonalite host mush and tonalite enclave; boundary defined by difference in abundance of acicular apatite inclusions in enclave (high) vs host rock (low). (d) Higher magnification image of the biotite shown in (c) displaying acicular rutile on only one side of boundary, suggesting that the crystallization rate was faster than the diffusion rate of titanium across the contact.

groundmass plagioclase laths, unaltered rounded clinopyroxene, lower abundances of hornblende, lower quartz (10 %), and very high amounts of apatite and Fe–Ti oxide inclusions. Some have inclusions of pyroxene, Fe–Ti oxide, and apatite throughout, whereas in others these inclusions are restricted to rims. Acicular apatite inclusions within groundmass plagioclase occur in much higher abundance than in the other magmatic enclave groups. Group 3 enclaves have to lowest silica content (~55 %) and are classified as pyroxene hornblende quartz diorite.

## Textures at unit boundaries

Thin sections that captured contacts between units reveal the petrographic nature of boundaries between magmatic enclaves and hosts, dykes and hosts, and major host units. Consistent with field observations, the contacts are almost always irregular at the thin-section scale and chilled margins are absent in all examined samples (e.g. Fig. 9a). Compared with their enclosing hosts, in magmatic enclaves (1) the grain size is always finer with the exception of plagioclase phenocrysts, which are approximately the same size, (2) major minerals such as plagioclase are generally more rounded or anhedral, (3) hornblende is more abundant, and higher amounts of hydrous minerals (biotite and hornblende) occur proximal to the boundary with hosts (Fig. 9b).

In addition to the grain size distinction, enclave–host rock boundaries in thin sections are usually defined by the appearance of fine-grained inclusions (apatite and Fe–Ti oxides) on the enclave side of the contact but not the host side. Individual minerals that crystallized along this contact can therefore be identified—such as biotite that contains titanite and rutile inclusions on one side of the crystal but not the other (Fig. 9c and d). Medium-grained minerals such as plagioclase and biotite are generally elongated parallel to the contact, indicating that shear was experienced at the boundary. In rare cases, interstitial liquid from one mush may have been

**Table 2:** Major and selected trace elemental compositions of representative samples taken from host rocks (biotite granite, enclave-rich tonalite, and enclave-poor tonalite).

| | Sample unit | | | | | | | | |
|---|---|---|---|---|---|---|---|---|---|
| | 71302 (BG) | 160704A (BG) | 0621B (BG) | 71602 (ERT) | 16070905 (ERT) | 71406 (ERT) | 71404 (EPT) | 16070901 (EPT) | 16070902 (EPT) |
| *Major elements (wt%)* | | | | | | | | | |
| $SiO_2$ | 76·02 | 73·77 | 77·04 | 56·73 | 58·76 | 67·99 | 59·98 | 62·59 | 61·08 |
| $Al_2O_3$ | 12·25 | 13·52 | 12·0 | 16·32 | 15·89 | 15·51 | 16·74 | 16·29 | 16·47 |
| $Fe_2O_3^T$ | 1·05 | 2·00 | 1·53 | 6·57 | 8·73 | 3·77 | 6·02 | 5·15 | 6·26 |
| MnO | 0·011 | 0·036 | 0·018 | 0·123 | 0·153 | 0·068 | 0·102 | 0·098 | 0·106 |
| MgO | 0·25 | 0·71 | 0·13 | 4·35 | 2·53 | 1·46 | 3·32 | 2·59 | 3·17 |
| CaO | 0·47 | 1·49 | 0·60 | 6·90 | 4·41 | 3·50 | 5·75 | 4·47 | 5·57 |
| $Na_2O$ | 2·26 | 3·87 | 3·84 | 4·28 | 4·81 | 4·84 | 4·39 | 4·40 | 4·82 |
| $K_2O$ | 6·51 | 3·80 | 3·96 | 1·11 | 1·93 | 1·31 | 1·42 | 1·87 | 1·30 |
| $TiO_2$ | 0·168 | 0·30 | 0·149 | 1·038 | 1·209 | 0·592 | 1·002 | 0·829 | 1·017 |
| $P_2O_5$ | 0·03 | 0·06 | 0·02 | 0·17 | 0·64 | 0·13 | 0·21 | 0·19 | 0·24 |
| LOI | 0·44 | 0·73 | 0·39 | 1·49 | 0·90 | 0·93 | 1·01 | 1·20 | 0·51 |
| Total | 99·46 | 100·3 | 99·7 | 99·08 | 99·97 | 100·1 | 99·94 | 99·68 | 100·5 |
| *Trace elements (ppm)* | | | | | | | | | |
| Rb | 91 | 104 | 76 | 28 | 38 | 24 | 41 | 55 | 28 |
| Sr | 183 | 131 | 63 | 508 | 435 | 303 | 456 | 384 | 412 |
| Ba | 791 | 262 | 396 | 265 | 479 | 400 | 329 | 563 | 343 |
| Y | 8 | 14 | 20 | 18 | 33 | 17 | 17 | 17 | 19 |
| Zr | 99 | 111 | 155 | 91 | 381 | 191 | 202 | 190 | 248 |
| Hf | 2·8 | 3·3 | 4·3 | 2·1 | 7·5 | 4·2 | 4·6 | 4·3 | 5·5 |
| Nb | 2 | 5 | 3 | 8 | 13 | 5 | 7 | 6 | 8 |
| Ta | 0·4 | 0·9 | 0·3 | 0·6 | 0·7 | 0·3 | 0·5 | 0·6 | 0·5 |
| La | 16·4 | 22·5 | 30·3 | 20·5 | 35·6 | 24·8 | 22·4 | 24·6 | 25·9 |
| Ce | 30·1 | 48·6 | 64·7 | 41·5 | 80·6 | 48·7 | 46·2 | 50·5 | 53·3 |
| Pr | 2·8 | 4·1 | 6·43 | 4·57 | 9·29 | 5·05 | 5·07 | 5·36 | 5·69 |
| Nd | 9·1 | 14 | 24 | 19 | 38·1 | 19·8 | 19·5 | 20·3 | 22·1 |
| Sm | 1·5 | 2·5 | 4·6 | 4·1 | 8·3 | 3·9 | 4·1 | 4 | 4·8 |
| Eu | 0·63 | 0·53 | 0·5 | 1·58 | 2·64 | 1·08 | 1·37 | 1·27 | 1·52 |
| Gd | 1·1 | 2·3 | 3·9 | 3·8 | 7·6 | 3·8 | 3·7 | 3·5 | 4·5 |
| Tb | 0·2 | 0·4 | 0·6 | 0·6 | 1·2 | 0·6 | 0·6 | 0·6 | 0·7 |
| Dy | 1·1 | 2·3 | 3·7 | 3·7 | 6·7 | 3·4 | 3·3 | 3·3 | 3·8 |
| Ho | 0·2 | 0·5 | 0·7 | 0·7 | 1·2 | 0·6 | 0·6 | 0·6 | 0·7 |
| Er | 0·8 | 1·5 | 2 | 2 | 3·3 | 1·8 | 1·9 | 1·8 | 2·1 |
| Tm | 0·13 | 0·23 | 0·3 | 0·31 | 0·44 | 0·25 | 0·27 | 0·25 | 0·28 |
| Yb | 0·9 | 1·7 | 2 | 1·9 | 2·8 | 1·6 | 1·7 | 1·7 | 1·9 |
| Lu | 0·15 | 0·28 | 0·3 | 0·28 | 0·41 | 0·23 | 0·25 | 0·25 | 0·27 |
| Th | 16·6 | 21·8 | 8·6 | 3·5 | 4·9 | 3·5 | 5 | 6 | 4·8 |
| U | 1·6 | 6 | 1·5 | 1·1 | 1·6 | 1·1 | 1·4 | 1·3 | 1·3 |

BG, biotite granite; EPT, enclave-poor tonalite; ERT, enclave-rich tonalite; $Fe_2O_3^T$, total Fe reported as $Fe_2O_3$; LOI, loss on ignition.

displaced and incorporated into an adjacent mush. For example, interstitial potassium-feldspar and fine-grained muscovite occur in the enclave-poor tonalite immediately adjacent to the boundary with the biotite granite whereas these minerals are otherwise absent in the enclave-poor tonalite unit.

## WHOLE-ROCK AND MINERAL CHEMISTRY

### Methods

To characterize major and trace element compositions, samples of all main rock units, the diorite sill and both mafic and felsic dyke samples were chosen for inductively coupled plasma mass spectrometry (ICP-MS) analysis, and 12 thin sections were analyzed using an electron microprobe micro-analyzer (EPMA) to determine the compositions of major minerals. Analytical methods are set out in Supplementary Data Electronic Appendix 3. Complete datasets and geochemical diagram are provided in Supplementary Data Electronic Appendices 4 and 5.

### ICP-MS major and minor geochemistry

Geochemical analyses of representative rock samples—a subset of those given in the Electronic Appendices—are shown in Tables 2 and 3, while Harker diagrams and trace element diagrams of all analysed rocks are given in Figs 10 and 11. As shown in Supplementary Data Electronic Appendix 5, all mingled units plot in the calc-alkaline fields of both the AFM ternary plot and the Th–Hf–Ta diagram of Pearce (1982).

On Harker diagrams most of the major element oxides form tight trends, many with linear, negative slopes (Fig. 10). The most silica-poor samples (<54 wt%) are from the diorite sill, whereas the mafic dykes and enclaves have silica contents between 54 and 59 wt%, overlapping with the more silica-poor host tonalites. The enclaves are, however, always more

**Table 3:** Major and selected trace elemental compositions of representative samples of magmatic enclaves, dykes and sill

| Sample unit | 71410 (G1) | 72802B (G2) | 71412 (G2) | 72804D (G3) | 72802C (G3) | 71401 (T dk) | 160705A (Qd dk) | 72001A (DS mrg) | 72001B (DS cntr) | 71601 (D dk) |
|---|---|---|---|---|---|---|---|---|---|---|
| *Major elements (wt%)* | | | | | | | | | | |
| $SiO_2$ | 59·22 | 57·27 | 57·64 | 54·08 | 55·66 | 59·51 | 57·34 | 53·24 | 51·15 | 53·58 |
| $Al_2O_3$ | 16·19 | 16·1 | 15·6 | 16·16 | 16·56 | 16·3 | 16·16 | 15·92 | 16·34 | 16·58 |
| $Fe_2O_3^T$ | 6·12 | 7·88 | 7·33 | 10·19 | 8·69 | 5·7 | 7·58 | 11·09 | 11·66 | 10·76 |
| MnO | 0·149 | 0·123 | 0·115 | 0·143 | 0·135 | 0·134 | 0·174 | 0·187 | 0·176 | 0·148 |
| MgO | 3·9 | 3·56 | 4·65 | 4·17 | 4·39 | 2·59 | 4·14 | 4·01 | 4·42 | 3·66 |
| CaO | 2·0 | 5·9 | 6·5 | 5·86 | 6·81 | 5·79 | 5·68 | 5·91 | 6·06 | 5·82 |
| $Na_2O$ | 4·93 | 4·43 | 4·08 | 4·02 | 4·05 | 5·36 | 3·61 | 3·96 | 4·12 | 4·39 |
| $K_2O$ | 1·79 | 1·76 | 1·23 | 1·51 | 1·4 | 1·61 | 1·81 | 1·8 | 2·01 | 1·0 |
| $TiO_2$ | 0·90 | 1·65 | 1·2 | 2·50 | 1·79 | 0·69 | 1·45 | 2·51 | 2·59 | 2·49 |
| $P_2O_5$ | 0·17 | 0·38 | 0·23 | 0·48 | 0·4 | 0·18 | 0·27 | 0·67 | 0·62 | 0·66 |
| LOI | 1·23 | 0·89 | 0·67 | 0·83 | 0·71 | 0·73 | 1·99 | 0·89 | 1·62 | 0·14 |
| Total | 100 | 99·95 | 99·25 | 99·94 | 100·6 | 98·59 | 100·2 | 100·2 | 100·8 | 99·23 |
| *Trace elements (ppm)* | | | | | | | | | | |
| Rb | 46 | 55 | 30 | 39 | 42 | 24 | 60 | 63 | 38 | 5 |
| Sr | 352 | 446 | 385 | 496 | 547 | 419 | 446 | 527 | 595 | 282 |
| Ba | 487 | 280 | 241 | 248 | 285 | 437 | 1462 | 647 | 401 | 143 |
| Y | 35 | 22 | 21 | 20 | 26 | 27 | 22 | 28 | 29 | 664 |
| Zr | 160 | 172 | 140 | 218 | 184 | 96 | 235 | 340 | 267 | 26 |
| Hf | 4·2 | 4·2 | 3·4 | 4·6 | 4·4 | 2·7 | 5·1 | 6·5 | 5·6 | 0·39 |
| Nb | 9 | 12 | 8 | 17 | 10 | 5 | 9 | 18 | 19 | 21 |
| Ta | 0·7 | 1 | 0·8 | 1·3 | 0·9 | 0·5 | 0·6 | 1·3 | 1·3 | 6·2 |
| La | 28·6 | 27·9 | 19·9 | 24·4 | 30·8 | 39·4 | 24·2 | 30·2 | 29·1 | 0·9 |
| Ce | 61·2 | 60·7 | 42·8 | 54·2 | 68 | 79·2 | 54·5 | 69·2 | 67·4 | 31·6 |
| Pr | 7·52 | 7·15 | 5·08 | 6·52 | 7·73 | 9·02 | 6·14 | 8·11 | 8·01 | 71·7 |
| Nd | 29·1 | 27·3 | 19·5 | 26·5 | 28·2 | 33·6 | 23·9 | 34·4 | 33·3 | 8·67 |
| Sm | 6·6 | 5·9 | 4·4 | 5·4 | 5·6 | 7 | 5·1 | 8 | 7·8 | 35·8 |
| Eu | 1·39 | 1·59 | 1·28 | 1·61 | 1·77 | 1·27 | 1·49 | 2·75 | 2·65 | 7·3 |
| Gd | 5·9 | 5·1 | 4 | 5·1 | 5·2 | 6 | 4·7 | 7·3 | 7·1 | 2·36 |
| Tb | 1 | 0·8 | 0·6 | 0·8 | 0·8 | 1 | 0·8 | 1·1 | 1·1 | 6·6 |
| Dy | 6·4 | 4·5 | 3·8 | 4·3 | 5·1 | 5·3 | 4·3 | 6·1 | 6·1 | 1 |
| Ho | 1·3 | 0·9 | 0·7 | 0·8 | 0·9 | 1 | 0·8 | 1·2 | 1·1 | 5·3 |
| Er | 3·8 | 2·3 | 2 | 2·3 | 2·7 | 2·8 | 2·4 | 3·1 | 3 | 1 |
| Tm | 0·58 | 0·36 | 0·31 | 0·32 | 0·41 | 0·42 | 0·33 | 0·41 | 0·4 | 2·8 |
| Yb | 3·8 | 2·4 | 2·1 | 2·2 | 2·7 | 2·6 | 2·3 | 2·6 | 2·6 | 0·38 |
| Lu | 0·57 | 0·33 | 0·3 | 0·32 | 0·4 | 0·41 | 0·33 | 0·4 | 0·38 | 2·5 |
| Th | 4·5 | 5·2 | 4·3 | 3·5 | 5·8 | 4·4 | 7·2 | 3·3 | 3·7 | $<$ 0·4 |
| U | 1·2 | 1·4 | 1·2 | 1·2 | 1·6 | 1·2 | 2·7 | 1·3 | 1·1 | 3 |

G1–G3, magmatic enclave Group 1–3; T dk, broken-up tonalite dyke from detailed map area; Qd dk, pair of parallel quartz diorite dykes from northernmost part of map area; DS mrg, margin of diorite sill; DS cntr, center of diorite sill; D dyke, thin broken-up diorite dyke.

mafic than their immediate hosts. The enclave-poor and enclave-rich tonalites have similar major element chemistries except for a sample of enclave-rich tonalite in the detailed map area (Fig. 5; Table 2, sample 71406). This sample displayed markedly more evolved chemical composition. Relative to their intermediate host rocks, magmatic enclaves show similar ranges in $Al_2O_3$, $P_2O_5$ and alkalis, and mostly higher amounts of MgO, $TiO_2$, and $Fe_2O_3^T$.

For the Wild Unit rocks, there is a general trend of decreasing Sr, Ti, and Nb with increasing $SiO_2$, consistent with plagioclase and hornblende fractionation, with more of a scatter in elements compatible with plagioclase and biotite (Ba and Sr) and a tighter trend in Ti, which is compatible with hornblende. Enclave-poor tonalite samples display a narrow range in $SiO_2$ compared with the enclave-rich tonalite (58–63 wt% and 56–68 wt%, respectively), and similarly show a more restrictive range in most trace elements.

Enclaves and host rocks (enclave-poor tonalite, enclave-rich tonalite and biotite granite) display similar abundances of incompatible elements (e.g. Rb, Ga), compatible elements (e.g. Sr, Y), and rare earth elements (REE). When normalized to chondrite compositions, all groups show similar REE patterns (Fig. 11). They are characterized by enrichment in light REE (LREE; 50–150 times chondrite) and flat heavy REE (HREE) patterns. Apart from the granites and a Group 1 magmatic enclave, the analysed rocks do not display Eu anomalies. All units display enrichment of large ion lithophile elements (LILE; K, Rb, and Ba) relative to high field strength elements (HFSE; Ta to Yb) and Ta and Nb are enriched 2–7 times relative to mid-ocean ridge basalt (MORB) in all units. When normalized to average continental crust (Taylor & McLennan, 1985), most incompatible elements show values close to those for average continental crust, except for a slight depletion in LILE.

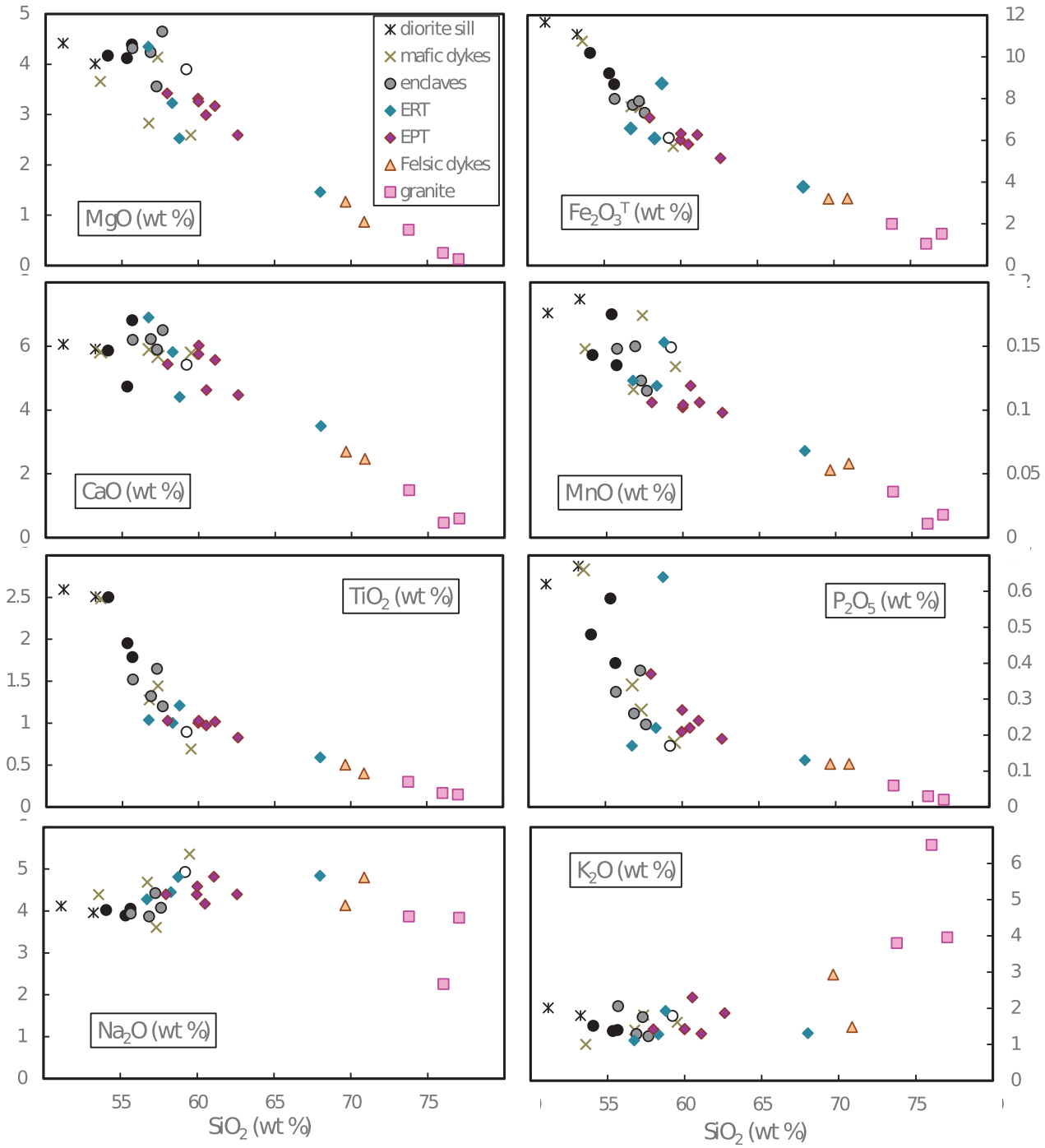


**Fig. 10.** Major element Harker diagrams for rocks of the Wild Unit.

## Plagioclase and pyroxene compositions

Based on petrography, plagioclase and pyroxene are interpreted to be the earliest minerals to have crystallized in all units and thus have the potential to record changing crystallization environments. In thin-section samples from the main lithological units, spot analyses of fine-grained groundmass crystals and cores and rims of phenocrysts were carried out to investigate their relationships. All data are available in Supplementary Data Electronic Appendix 6.

Summary results are displayed in Fig. 12. The plagioclase compositions are consistent with the major element geochemistry in that the more mafic units have the higher An contents. In general, the rims of plagioclase in matrix and ground mass are more sodic than their respective cores, and the more mafic units show a wider

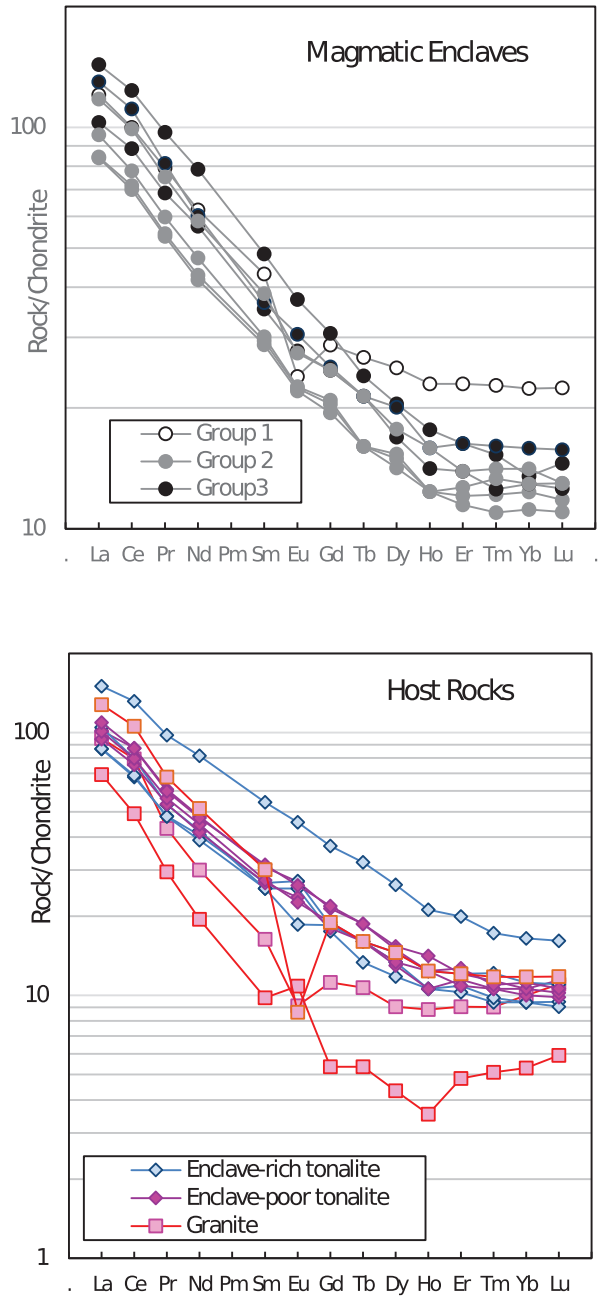


**Fig. 11.** Chondrite-normalized REE patterns for host rocks and enclaves of the Wild Unit.

range of compositions. The clinopyroxene compositions of the rocks, however, do not show such consistent correlations.

Core and rim analyses by EPMA were conducted on plagioclase on either side of an interface between the enclave-rich tonalite (sample core 2 qdx) and enclave-poor tonalite (sample core 2 qd) units. A wide range in core compositions is observed in single thin sections for both units, with a range of $An_{44–26}$ in the enclave-poor tonalite and $An_{33–19}$ in the enclave-rich tonalite. Plagioclase cores displaying resorption textures are sometimes more and sometimes less An-rich than their corresponding rims. A narrow rim compositional range of $An_{19–21}$ is observed in the enclave-rich tonalite units. These results point to different histories of the two units and a lack of chemical exchange.

### *Contrasting compositional trends within crystal populations*

The occurrence of crystal populations with contrasting compositions in the same rock, particularly plagioclase, has been reported in previous studies on magma mingling and magmatic enclave formation (e.g. Wiebe, 1968; Astbury *et al.*, 2016). Two mottled plagioclase phenocrysts displaying distinct core compositions occur in the same thin section from a Group 2

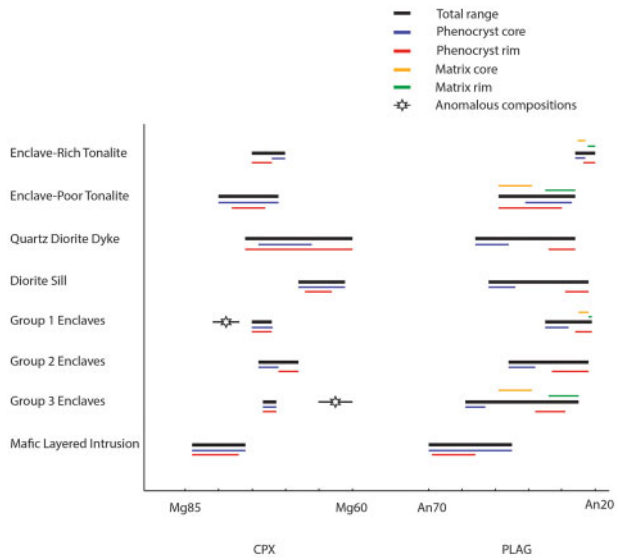


**Fig. 12.** Summary plot displaying range in composition of pyroxene and plagioclase in major units. Lines with stars represent anomalous mineral compositions that are unusual compared with the rest of the rock such as: (1) $Mg_{80–76}$ core of corroded pyroxene in a Group 1 enclave, and (2) pyroxene in Group 3 enclave with an $Mg_{65}$ core and $Mg_{60}$ rim.

magmatic enclave (Fig. 13a; sample 72804A). The crystals have a similar compositional range of $An_{50–20}$; however, the core compositions of the two crystals are on opposite ends of that range, with one core of $An_{50}$ and the other of $An_{23}$. The two crystals also display distinctly different trends from core to rim, as illustrated by the profiles in Fig. 13.

As documented in Supplementary Data Electronic Appendix 6, a difference in compositional trends within plagioclase phenocrysts is also observed in the enclave-poor tonalite sample (71408). One mottled phenocryst displays a steady reverse zoning trend to more primitive compositions from core to rim, with a core value of $An_{23}$ and a rim value of $An_{33}$. A second crystal displays a more complicated trend of initial reverse zoning from core ($An_{33}$) to intermediate parts of the crystal ($An_{40}$) followed by a normal compositional evolution toward the rim ($An_{33}$).

In addition to plagioclase, there are zoned pyroxenes with outlier compositions. Several zoned pyroxene in a Group 1 magmatic enclave (sample 71410) display anomalous core compositions ($Mg_{80–76}$) compared with the average compositional range of pyroxene in the same thin section ($Mg_{73–71}$). Similarly, an anomalous pyroxene from a Group 3 magmatic enclave displays more evolved compositions ($Mg_{60}$ core, $Mg_{65}$ rim) compared with neighbouring analysed pyroxene ($Mg_{73}$). These anomalous compositions are represented by star symbols in Fig. 12.

### *Mottled or resorbed plagioclase*

Some plagioclase grains in both Group 1 and Group 2 magmatic enclaves are composed of two zones: a mottled andesine ($An_{32}$) core, and an oligoclase ($An_{22}$) overgrowth or rim (Fig. 13). The abrupt peaks and valleys in An content across the traverses correlate with patchy zoning that is seen in both crossed polar microscopy and backscatter images. The zoning indicates that the earliest crystallizing phase was andesine and it was later overgrown by oligoclase. The mottled appearance of the andesine cores probably records a period of partial resorption of the core (Wiebe, 1968). In the core regions ($An_{32}$) of some crystals there are small clinopyroxene inclusions, which, based on similar extinction angles, are corroded remnants of original coarser-grained pyroxene. The inclusions become more Fe-rich towards the rim of the enclosing plagioclase phenocryst ($Mg_{74} \rightarrow Mg_{71}$). Rapid decompression of a magma has been proposed as a process that can lead to resorption of early forming minerals (Yücel *et al.*, 2014).

Plagioclase grains displaying disequilibrium textures were also examined in samples taken from a quartz diorite dyke (location A in Fig. 3; Fig. 4) that broke up into rounded magmatic globules at its margins; the range of $An_{50–30}$ seen in two plagioclase phenocrysts is close to that observed in Group 3 magmatic enclave phenocrysts (Fig. 12). Oscillations in the range $An_{30–50}$ occur in the mottled regions of both crystals and represent the core and overgrowth regions, respectively. Some plagioclase grains are mottled across their entirety. A second plagioclase shows early resorption of an oligoclase core ($An_{30}$), followed by prolonged crystallization of labradorite ($An_{50}$) beginning midway through the traverse and finally crystallization of an oligoclase rim ($An_{30}$). Pyroxene inclusions are restricted to the mottled oligoclase core and rims.

### *Zoned pyroxene*

One analysis from a Group 1 magmatic enclave is of a clinopyroxene that displays three compositional

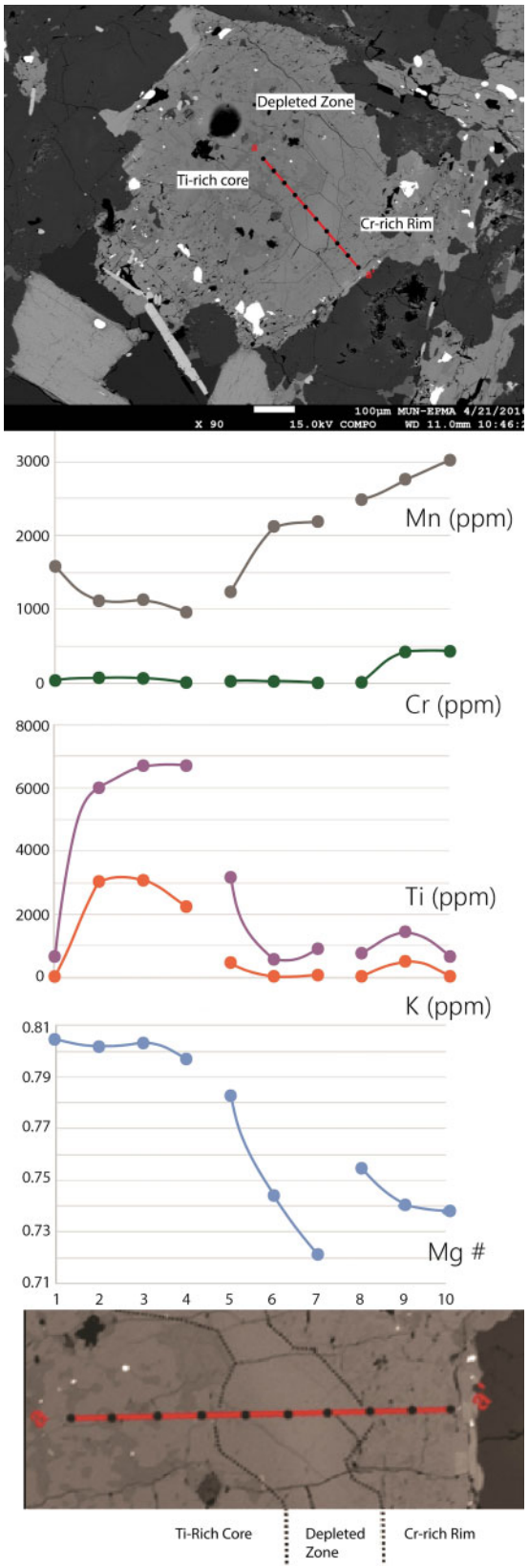


**Fig. 13.** EPMA traverses across two mottled plagioclase phenocrysts from single thin section of Group 2 enclave. Traverses show markedly different compositional trends from core to rim.

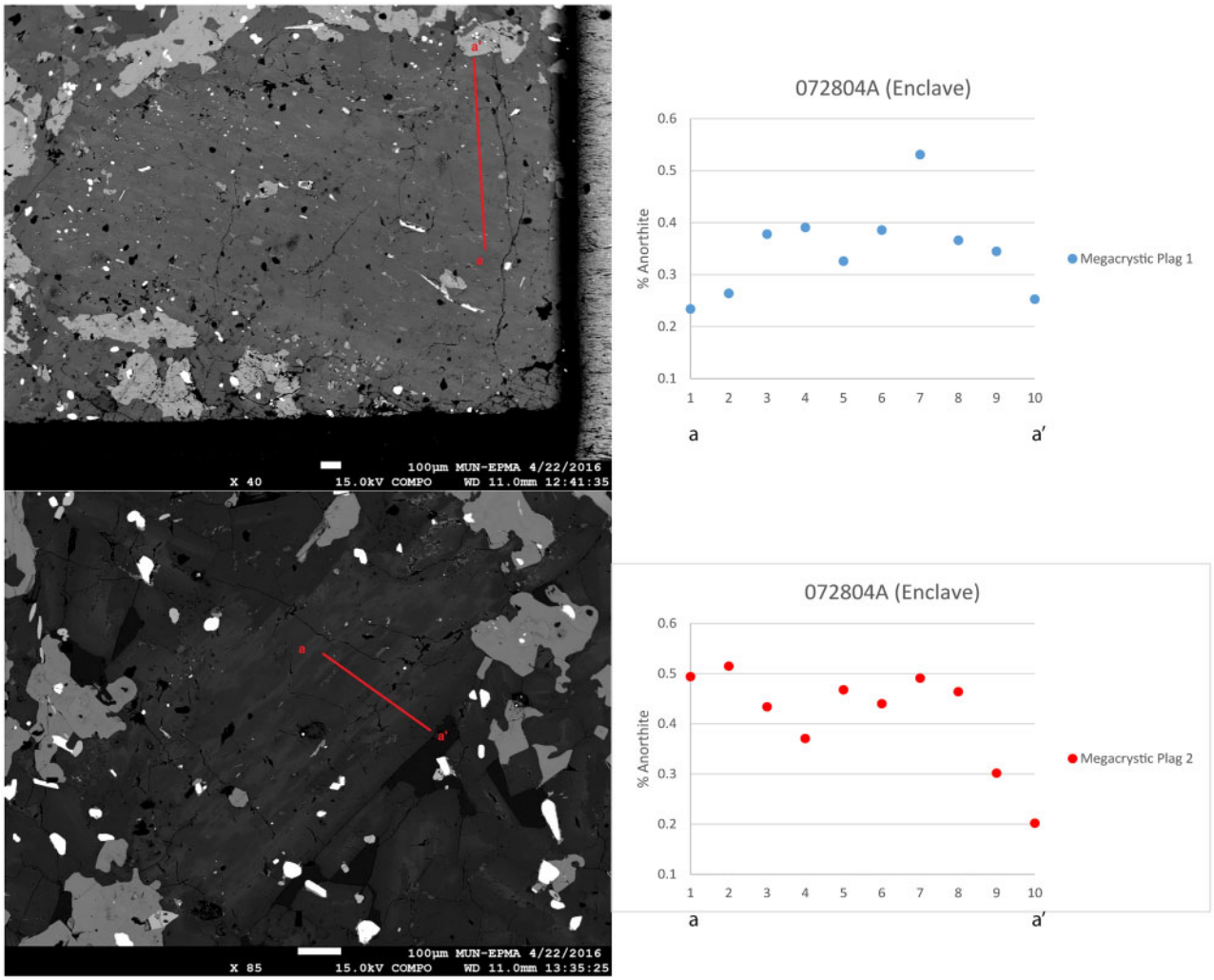


**Fig. 14.** Backscatter images and analysis by EPMA of a Group 1 enclave clinopyroxene. A 10-point traverse was conducted from core (a) to rim (a′). The core is titanaugite and contains Ti-bearing minerals such as ilmenite (oxide minerals are white in the backscatter images). The compositional trends suggest a four-stage history: (1) crystallization from a Ti-rich alkaline magma; (2) fractionation of alkaline magma to form the middle zone; (3) late crystallization from a more mafic Cr-rich magma; (4) incorporation into tonalite crystal mush.

zones corresponding to crystallization under different conditions: a Ti-rich core, an intermediate zone depleted in Mg and Ti, and a Cr-rich rim (Fig. 14). The core is titanaugite, a mineral generally derived from alkaline magmas (Leung, 1974). In the depleted zone, there is a gradual decrease from $Mg_{81}$ to $Mg_{72}$ away from the core, until a sudden increase to $Mg_{76}$ occurs across a visible boundary close to the rim. At the same point, Cr increases significantly to nearly 500 ppm. Similarly examined were several zoned clinopyroxene grains from the quartz diorite dyke (location A in Fig. 3; Fig. 4). One pyroxene oscillates between $Mg_{76}$ and $Mg_{71}$ from core to rim, suggesting either changing pressures or minor mafic recharge (Streck, 2008). The increase in Mg # towards the rim of the crystal is accompanied by a significant rise in Cr by almost 400 ppm and in Mn by nearly 1000 ppm.

## U–PB ZIRCON GEOCHRONOLOGY

### Methods

Euhedral zircons were picked for analysis from four samples: biotite granite and enclave-poor tonalite from within the detailed field area (Fig. 5), the diorite sill and the chilled diorite dyke (Fig. 3). Analytical methods, which include the chemical abrasion thermal ionization mass spectrometry (CA-TIMS) technique, are set out in Supplementary Data Electronic Appendix 3. U–Pb zircon data are presented in Supplementary Data Electronic Appendix 7.

### Results

#### *Biotite granite*

Clear euhedral prismatic zircons that range in size from 50 to 100 μm were obtained from the biotite granite unit (sample BG06-21A). Three of the most euhedral grains were selected for analysis. Cathodoluminescence (CL)

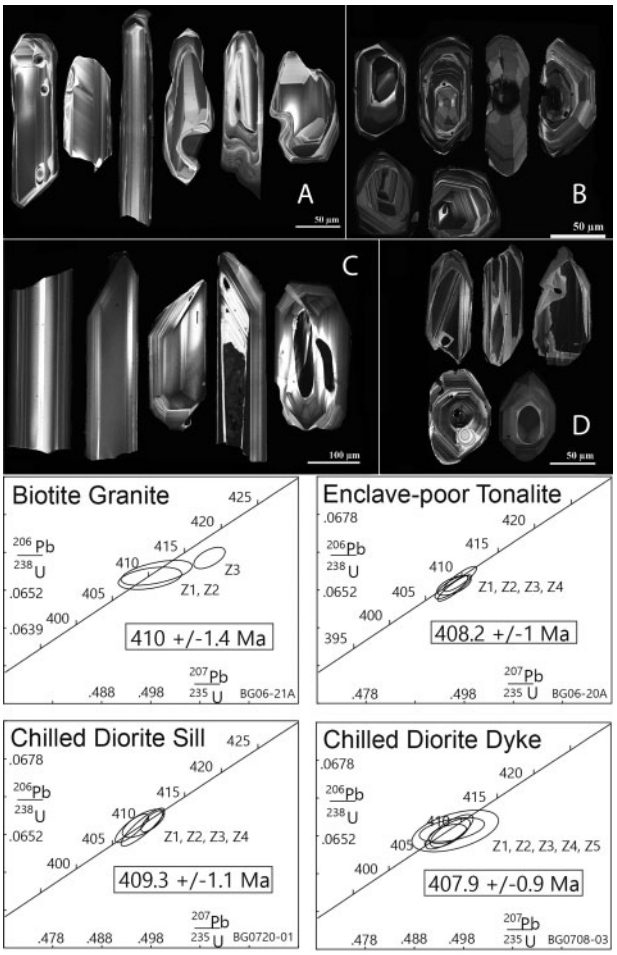


**Fig. 15.** Above: cathodoluminescense images of zircon crystals representative of the type analyzed from four sample from the Wild Unit. Below: concordia diagrams of U–Pb results of zircon analyses from corresponding samples. Error ellipses are at the 2σ level.

imaging reveals complicated igneous growth zoning in most of the crystals (Fig. 15a). In many cases, multiple growth zones truncate previous zones. Some crystals display bright cores and dark rims whereas other grains contain darker cores and bright rims. Two analyzed grains show significant overlap and yield a concordant $^{206}Pb/^{238}U$ age of 410 ± 1·4 Ma. A third grain (Z3) displays evidence of an older component and was therefore excluded during age calculation of this rock.

### *Enclave-poor tonalite*

The enclave-poor tonalite (sample BG06-20A) yielded clear subhedral prismatic to elongate zircons. Four of the most euhedral grains, ranging in size from 50 to 100 μm, were selected for analysis. All crystals display igneous growth zoning, some with dark cores and lighter rims. Oscillatory zoning is observed through the entirety of some crystals and is restricted to particular regions of other grains. One imaged zircon displays evidence of partial resorption of the core followed by multiple sequences of overgrowth (Fig. 15b). All fractions tightly overlap and yield a concordant $^{206}Pb/^{238}U$ age of 408·2 ± 1 Ma.

### *Diorite sill*

The diorite sill (sample 72001) yielded abundant large (300–500 μm) elongate to prismatic zircons. Both cracked or broken grains and euhedral zircons displaying grain tips were observed (Fig. 15c). The grains generally display simple igneous zoning in CL imaging. Several grains display more complicated zoning patterns but these are not representative of the majority. All four analyzed fractions tightly overlap and yield a concordant $^{206}Pb/^{238}U$ age of 409 ± 1·1 Ma.

### *Chilled diorite dyke*

Clear euhedral elongate to prismatic zircons were obtained from a diorite dyke (sample 16070803) near the eastern boundary of the field area (Fig. 3). This minor intrusion is the only unit in the study area to display a straight chilled margin and is therefore interpreted to be the youngest unit in the study area. Five of the most euhedral representative zircons were selected for analysis. CL imaging reveals that many of the grains display complicated igneous zoning (Fig. 14d). Grains generally contain dark embayed core regions suggesting resorption, along with lighter rim regions. A concordant $^{206}Pb/^{238}U$ age of 407·9 ± 0·9 Ma was determined from all tightly overlapping fractions.

## DISCUSSION

The subject of this study, the Wild Unit of the Fogo Batholith, consists of mostly intermediate (quartz diorite to tonalite) rocks exposed in a cove toward the NE boundary of the Batholith (Fig. 2). We interpret the rocks to represent a small crystal mush reservoir that existed as an open system at shallow crustal depth and that preserves evidence of the last stages of dynamic intrusion before final solidification. That the principal units interacted as mushes is indicated by field relations and petrographic textures. Intermediate magmas have a wide temperature interval between liquidus and solidus (Stern *et al.*, 1975) and can therefore exist as crystal mushes for a relatively long period, so a moderate temperature difference between units at the time of emplacement cannot be ruled out. In the sections below, we present an emplacement model that is based primarily on field and petrographic relationships, given that the U–Pb zircon ages of all major units are close enough that their relationship cannot be distinguished by geochronology alone, and that zircon can retain a record spanning multiple emplacement and crystallization events (Miller *et al.*, 2007).

### Tectonic setting

The 7 km thick gabbro–diorite–tonalite–granite Fogo Batholith is interpreted to have intruded during widespread strike-slip deformation that affected Central

Newfoundland in the Silurian–Devonian; in particular, during dextral–transtensional movement along the Dog Bay Line in the early Acadian orogeny (Williams , 1993; Currie, 2003; Pollock *et al.*, 2007; Fig. 1). New U–Pb zircon ages from the Wild Unit correlate with those from previous studies of the Fogo Batholith (Aydin, 1994) and those of nearby Early Devonian intrusions (Fig. 1). This tectonic event would have disrupted the lithosphere, allowing decompression melting of the mantle to produce basalts and crustal anatexis to produce felsic magmas (Currie, 2003), and also promoted deformation-enhanced segregation of magmas from their source (Rutter & Neumann, 1995; Petford *et al.*, 2000). Fogo Batholith magmas are probably hybrids of mantle and crustal melts (e.g. Edmonds *et al.*, 2019), but because the pre-existing accreted arc crust is at most 150 Myr older than the Fogo Batholith (Colman-Sadd *et al.*, 2000) it would be challenging to calculate relative amounts of these sources with isotopic analysis.

## Emplacement model for the Wild Unit

Miller *et al.* (2011) proposed that incremental construction of plutons is achieved as new pulses of magma are injected into relatively weak, melt-rich regions within a magma mush. Following this model and based on evidence that will be presented in detail below, we suggest the following history for the Wild Unit.

The enclave-poor tonalite intruded in several pulses as a relatively crystal-poor slurry into a shallow-level magma chamber underneath a mostly solidified granite roof. A granite roof is indicated by the facts that granite is the dominant rock immediately inland of the coastal exposures and it overlies the tonalite in a few places (Fig. 3). Features such as metasedimentary xenoliths and miarolitic cavities within the granite at some locations imply that reservoir storage occurred close to the walls or roof of a pluton at shallow crustal depths.

The crystal load in the tonalite settled downward, perhaps deposited in gravity currents, and some melt may have erupted (Barnes *et al.*, 2019), leaving weak melt-rich regions, which were later intruded by similarly crystal-poor but enclave-rich tonalite and by diorite. The largest intrusion produced the diorite sill, and smaller intrusions produced layers ('one-sided chilled dyke' in Fig. 3) or broke up into magmatic enclaves. All these later intrusions solidified with little large-scale motion after injection, although there was probably relative motion between some of the magmatic enclaves and host tonalite crystal mushes. During these later intrusions, a largely crystalline slab of granite stoped off the roof and foundered, breaking up, into underlying mush (Fig. 5). In the process, it compressed underlying mush leading to ejection of relatively silica-rich melt (Table 2, sample 71406) and the swirling pattern of small enclaves seen in the centre of Fig. 5. Webber *et al.* (2015) interpreted a similar pattern in the Coastal Batholith, Chile, to indicate migration of melt and vigorous mixing.

As the region cooled and crystallized, the final intrusive activity occurred as dykes, some into relatively weak mush, so that there was some interaction of dyke and wall materials. Thin (5–20 cm wide) north-striking intermediate to granitic dykes cut across all units and display sharp chilled contacts suggesting that they intruded after complete solidification of the reservoir.

### *Intrusion of tonalite mushes and diorite sill*

We interpret the enclave-poor tonalite as forming as an open-system mush. While the enclave-poor tonalite was intruding, heat was supplied to the local system from the tonalite intrusions themselves and perhaps by nearby mafic intrusions. The intrusion of the 200 m wide troctolite–gabbro mafic layered sill located at the eastern end of the study area potentially represents an example of a late recharge event that took place close to the current interpreted shallow level. The sill displays an irregular chilled margin with the enclave-rich tonalite at its western end. Additionally, located a few kilometres to the east is a series of layered gabbros belonging to the Tilting Layered Suite (Aydin, 1994) that overlap in age with the rocks of the Wild Unit (409·8 ± 0·8 Ma for a pegmatite differentiate in a layered gabbro; Gorner, 2016). Together, these mafic intrusions may have provided the energy to prolong the lifetime of the tonalite crystal mush as well as produce resorption and reverse zoning in early forming plagioclase and pyroxene.

The enclave-poor tonalite is locally found underneath the enclave-rich tonalite, and it commonly surrounds small regions of enclave-rich tonalite (Fig. 3). This distribution of the units suggests that the enclave-rich tonalite was intruded into enclave-poor tonalite. Some contacts (Fig. 7) are steep, suggesting that the weak regions were pockets rather than a continuous layer. Whether the pockets were connected at a level higher than the current coastal erosion level is unknown; possibly not. Given the proximity of the interpreted granite roof, the magmatic layer cannot have been very thick and variations in thickness close to a cooling roof are not unexpected.

The elongated, disc-shaped geometry of the diorite sill suggests that it too was intruded into a localized pocket. Consequent compaction of tonalite mush and squeezing out of melt surrounding the diorite sill is indicated by pipe structures (Wiebe & Collins, 1998; Paterson, 2009; Fig. 8).

The different textures of the units, with much higher percentages of euhedral crystals in the enclave-poor tonalite than in the enclave-rich tonalite, suggest that crystal compaction occurred in the former and not the latter. The cumulate nature of the enclave-poor tonalite is consistent with the work of Barnes *et al.* (2019), who demonstrated that for three arc-related magmatic systems there was significant (~40 %) melt loss and crystal accumulation in the granitoid rocks.

Differences in the crystal chemistry between the units near contacts indicate that the mushes did not experience chemical exchange when the enclave-rich tonalite was intruded. However, the mafic contact between the tonalite mushes (Fig. 7) provides evidence of mobility of crystal packages and volatiles within the enclave-rich tonalite. Refractory minerals such as pyroxene may have been sheared out and deposited along the boundaries between the mobile enclave-rich tonalite and the more crystalline enclave-poor tonalite on emplacement.

### *Schlieren*

The smooth, curved contacts between the tonalite units indicates that both units were mushes when they came together; however, the different geometry of schlieren in the two tonalite units points to different intrusion styles. In the enclave-poor tonalite, schlieren are planar as they would be for flow in sheets or gravity currents in a dynamic open system. In the enclave-rich tonalite they are wrapped around or tail behind magmatic enclaves, suggesting shear segregation of mafic minerals or peeling off of enclave material in more localized flow, as magmatic enclaves moved (sank?) slowly in a more quiescent mush (Wiebe *et al.*, 2007).

### *Tilting*

As magmatic systems evolve, intrusions that might originally have been horizontal become tilted as further magma is introduced (e.g. Weibe *et al.*, 1996). The map of Fogo Island (Fig. 2) indicates that a significant part of the batholith is now tilted toward the present-day NW, although this is not evident in the NE. In Wild Cove East there is little evidence of post-emplacement tilting. The best evidence of relatively little tilting in the area is from the diorite sill (location B in Fig. 3): magmatic pipes in this unit (Fig. 8a) are near vertical. Further evidence of lack of significant tilting is found in a dotted line of millimetre-scale silicic segregations, which mark an approximately horizontal contour in the gently scalloped erosional top of the sill. We interpret this horizon to represent a flat boundary between the solidified top boundary region of the sill and a more mushy region through which the silicic segregations rose (e.g. Zavala *et al.*, 2011).

### *Estimates of emplacement crystallinity*

According to the review by Petford *et al.* (2000), most felsic plutons in the upper crust are emplaced with a crystallinity of $\leq$30 %. In the Wild Unit, we propose that the enclave-rich tonalites cooled rapidly upon emplacement at the current erosional level, and hence it is plausible that emplacement crystallinity can be estimated from the percentage of phenocrysts of early forming phases (plagioclase and pyroxene) that are euhedral or resorbed. Representative thin sections gave the quantity of these phenocrysts as 20 % in the enclave-rich tonalite and 15 %, 30 % and 35 % for magmatic enclaves of Group 1, 2 and 3 respectively. An emplacement crystallinity of 20 % for the enclave-rich tonalite is reasonable as such a mush would be mobile (e.g. Marsh, 2002). For the magmatic enclaves, the inferred emplacement crystallinity is correlated to composition, with the more mafic magmatic enclaves being more crystal-rich. This is consistent with the enclaves being at a similar temperature on emplacement.

Petrographic examination of enclave-poor tonalite showed that an estimated 50 % of crystals are euhedral, too high to represent emplacement crystallinity. This unit was probably affected by crystal settling and compaction (Barnes *et al.*, 2019), evidenced by the imbrication of plagioclase phenocrysts and the presence of schlieren (Marsh, 2002; Streck, 2008). Although they depend on the history of recharge and reheating, resorbed plagioclase cores arguable represent part of the original crystal cargo, which underwent resorption when they were emplaced into a lower-pressure environment. Resorbed cores in plagioclase make up a significant 15–20 % of the enclave-poor tonalite, suggesting that the original magma was not exceptionally crystal poor. Based on the petrography, it is not possible to make a reasonable estimate of emplacement crystallinity. Some of the euhedral crystals may have been present during emplacement and melt-rich magma may have been extracted, as the system was probably open during emplacement of the enclave-poor tonalite.

### *U–Pb zircon geochronology*

The four U–Pb zircon ages (Fig. 15) overlap within their uncertainties, covering a relatively short interval of 2 Myr. The order of oldest and youngest ages—$410 \pm 1{\cdot}4$ Ma for the biotite granite and $407{\cdot}9 \pm 0{\cdot}9$ Ma for the chilled diorite dyke—is consistent with the field relations. Field relations indicate that the diorite sill is the same age as the enclave-poor tonalite, which it intruded when they were both mushes. The geochronology gives an older age for the diorite sill, although the ages overlap within the calculated uncertainties. We acknowledge, however, particularly in light of textural evidence indicating a complex magmatic history, that zircons are likely to preserve this prior history, and the range of ages may be a better indication of the time spent in the crustal plumbing system than of individual emplacement times.

## Nature and formation of magmatic enclaves

Magmatic enclaves of the Wild Unit have ellipsoidal–rounded shapes, and the stretching direction of some is parallel to nearby flow fabric and/or schlieren in the host tonalite, indicating that they were transported—or perhaps deformed in place—while in a partially molten state within a crystal mush. For the assumed emplacement crystallinities in the host rock units (volume fractions $\geq$0·2), the mushes probably had a plastic rheology

with a yield strength (Fernandez & Barbarin, 1991; Wiebe *et al.*, 2007). If sinking did occur, magmatic enclaves located in particularly crystal-poor regions of the heterogeneous mush would presumably sink until they reached regions with higher crystal concentrations that had a sufficient yield strength to prevent sinking (Wiebe *et al.*, 2007).

Magmatic enclaves are mineralogically and texturally distinct from their hosts with little to no evidence of chemical exchange across their sharp boundaries (see Fig. 9). Three groups of magmatic enclaves are distinguished based on their mineral chemistry, composition, and crystallinity (Table 1). From Groups 1 to 3, magmatic enclaves have more euhedral crystals and change in general morphology from cuspate in Group 1, to elongated or stretched in Group 2, and to rounded in Group 3. These observations suggest that magmatic enclaves were progressively less deformable in the tonalite mushes: Group 2 magmatic enclaves has similar viscosities to their hosts, whereas Group 1 magmatic enclaves were weaker and Group 3 magmatic enclaves were stiffer.

The exact mechanisms for magmatic enclave formation are unknown, but they probably come about owing to a shear instability between the two magmas, either at a boundary between them or when a dyke-like injection into a slurry breaks up into rounded globules (Frost & Mahood, 1987; Wiebe & Collins, 1998). In the Wild Unit, different magmas clearly did inject at the emplacement level (Figs 5 and 6), and the margins of a metre-wide quartz diorite dyke show localized break-up into rounded globules (Fig. 4) so it is likely that some of the enclaves formed there. However, because Group 1 magmatic enclaves commonly occur amongst other populations, we infer that formation and mixing of magmatic enclaves happened at a deeper level in the magmatic system and that they were transported to the current level already enclosed in their hosts.

### Mineral evidence for changing physical and chemical environments

Mineral textures, such as mottled cores in plagioclase, record changes in the physical or chemical environments experienced by crystals during their histories (Chen *et al.*, 2009). Many of the plagioclase phenocrysts in both magmatic enclaves and host tonalite mushes display mottled or resorbed textures, and variations in chemical trends from core to rim for plagioclase within individual sections, suggesting that crystals experienced periods of normal growth in an undisturbed magma (reflected by normally zoned crystals) and periods of reheating and subsequent cooling, or growth from a hotter and more mafic melt (reversely zoned crystals). Generalized trends in the crystal zoning are shown in Fig. 12; however, there is significant heterogeneity within the units on different scales. In samples taken from different parts of the enclave-poor tonalite unit, some appear to be petrographically simple and others nearby show greater complexity, where plagioclase phenocrysts with different core compositions and chemical trends, including complex zoning or resorption, are seen juxtaposed on a thin-section scale. Magmatic enclaves also display heterogeneities at the mineral scale, as evidenced by anomalous clinopyroxene crystals with distinct zoning and compositions (Fig. 13).

Heterogeneity in temperature and/or chemical environments could be experienced by individual crystals during complex mixing events. For example, a fresh intrusion could disrupt the less crystalline components of a mush in the immediate vicinity of the intrusion to produce localized mixing and heat transfer, whereas mush nearby would be relatively undisturbed (Bergantz *et al.*, 2015). Some mineral-scale heterogeneities in overgrowth patterns in the enclave-poor tonalite might have arisen at the emplacement level, if the unit was formed during multiple influxes in an open system, as we suggest here. However, to account for large differences in phenocryst cores at the thin-section scale for magmatic enclaves and tonalite mushes, we infer that complex mixing processes, perhaps in an interleaved mafic and silicic geometry as outlined in the MASLI model (Weibe, 1996), took place at deeper levels in the crust.

To account for the emplacement of mushes that display large-scale homogeneity together with small-scale heterogeneity, Burgisser & Bergantz (2011) proposed that highly viscous crystal mushes in the mid-crust can be rapidly remobilized, or 'defrosted', as a result of reheating from below by fresh magmatic intrusions. In their model, rapid overturn creates strong mixing and can lead to the juxtaposition of crystals and magmatic material with contrasting chemistry, textures, and ages (Burgisser & Bergantz, 2011; Schleicher *et al.*, 2016).

The growth zoning seen in zircon (Fig. 15), a strongly refractory mineral, is consistent with textures observed in both plagioclase and pyroxene, indicating that it probably experienced complex histories involving displacement between multiple magmas or mushes during ascent through the crust (Storm *et al.*, 2012).

## CONCLUSIONS

U/Pb zircon geochronology of four units of the Wild Unit at the edge of the Fogo Island Batholith gave ages, with overlapping uncertainties, between 410 and 408 Ma, consistent with generation and emplacement during widespread transpressional deformation in Newfoundland during the Arcadian orogeny.

Magmatic systems, such as the one that produced the Fogo Island Batholith, are complex and dynamic, involving multiple pulses of different sorts of magma over length scales of tens of kilometers and timescales of a few million years. As observers, we typically see a single surface slice of the end product of all this overprinting activity, and untangling the history is challenging. In the Wild Unit, good exposure of the edge of the batholith at shallow levels provides an excellent

opportunity to observe evidence of the last magmatic activity frozen in place over a relatively short timescale. Detailed mapping allowed the sequence of events to be proposed, starting with pulses of crystal-poor magma, continuing with the interaction of crystal mushes, and finishing with the intrusion of dykes through crystalline rock. The presence of visually distinct although compositionally similar magmatic enclaves was of significant benefit in distinguishing rock units and revealing key facets of rheology and dynamics. The fact that most rocks spanned a narrow, intermediate compositional range is significant, in that the magmas interacted as slurries and mushes over a relatively large timescale without chilling.

Petrological examination suggested low emplacement crystallinity, whereas geochemical analyses and backscatter imaging of individual phenocrysts of plagioclase and pyroxene and CL imaging of zircon grains showed that these crystals had complex histories, involving changing chemical environments. Because such a level of complexity did not exist at the emplacement level—unit boundaries, even at the edges of the magmatic enclaves, are sharp with very little evidence of chemical exchange—this points to dynamic interactions deeper in the magmatic system. The observation that three types of magmatic enclaves, varying in composition and texture, were found in close proximity is another indication of the importance of mingling processes at deeper levels.

## FUNDING

This work was supported by the Hibernia Geophysics Fund at Memorial University.

## ACKNOWLEDGEMENTS

We thank our field assistant Emily Gorner, technicians Pam King and Wanda Alyward for help with sample preparation and analysis, and Neil Stapleton, from the Geoscience Publications and Information Section of the Geological Survey, Newfoundland and Labrador Department of Natural Resources, for assistance with maps. We also thank Calvin Miller for a thorough, thoughtful and very helpful review.

## SUPPLEMENTARY DATA

Supplementary data are available at Journal of Petrology online.

## REFERENCES

Abbott, R. N. (1989). Internal structures in part of the South Mountain batholith, Nova Scotia, Canada. *Geological Society of America Bulletin* **101**, 1493–1506.

Astbury, L. A., Petrelli, M., Arienzo, I., D'Antonio, M., Morgavi, D. & Perugini, D. (2016). Using trace element mapping to identify discrete magma mixing events from the Astroni 6 eruption. *AGU Fall Meeting 2016 Abstracts* V33E-3176.

Aydin, N. S. (1994). Physical characteristics of the Tilting Layered Suite, Fogo Island, Newfoundland. *South African Journal of Geology* **97**, 496–506.

Baird, D. M. (1958). *Fogo Island map-area, Newfoundland. Geological Survey of Canada. Memoir* **301**, 63.

Barnes, C. G., Werts, K., Memeti, V. & Ardill, K. (2019). Most granitoid rocks are cumulates: deductions from hornblende compositions and zircon saturation. *Journal of Petrology* **60**, 2227–2240.

Barriere, M. (1981). On curved laminae, graded layers, convection currents and dynamic crystal sorting in the Ploumanac'h (Brittany) subalkaline granite. *Contributions to Mineralogy and Petrology* **77**, 214–224.

Bergantz, G. W., Schleicher, J. M. & Burgisser, A. (2015). Open-system dynamics and mixing in magma mushes. *Nature Geoscience* **8**, 793–796.

Burgisser, A. & Bergantz, G. (2011). A rapid mechanism to remobilize and homogenize highly crystalline magma bodies. *Nature* **471**, 212–215.

Chen, B., Chen, Z. C. & Jahn, B. M. (2009). Origin of Mafic Enclaves from the Taihang Mesozoic Orogen, North China Craton. *Lithos* **110**, 343–358.

Claiborne, L. L., Miller, C. F. & Wooden, J. L. (2010). Trace element composition of igneous zircon: a thermal and compositional record of the accumulation and evolution of a large silicic batholith, Spirit Mountain, Nevada. *Contributions to Mineralogy and Petrology* **160**, 511–531.

Colman-Sadd, S. P., Hayes, J. P. & Knight, I. (2000). *Geology of the Island of Newfoundland.* Newfoundland Department of Mines and Energy, Geological Survey, Map **2000-30**.

Currie, K. L. (1997). *Fogo map-area, Newfoundland. Geological Survey of Canada Open File* **3466**.

Currie, K. L. (2003). Emplacement of the Fogo Island batholith, Newfoundland. *Atlantic Geology* **39**, 79–96.

de Saint Blanquat, M., Horsman, E., Habert, G., Morgan, S., Vanderhaeghe, O., Law, R. & Tikoff, B. (2011). Multiscale magmatic cyclicity, duration of pluton construction, and the paradoxical relationship between tectonism and plutonism in continental arcs. *Tectonophysics* **500**, 20–33.

Edmonds, M., Cashman, K. V., Holness, M. & Jackson, M. (2019). Architecture and dynamics of magma reservoirs. *Philosophical Transactions of the Royal Society of London, Series A* **377**, 20180298. 10.1098/rsta.2018.0298

Elliot, C., Dunning, G. & Williams, P. (1991). New U/Pb zircon age constraints on the timing of deformation in north–central Newfoundland and implications for early Paleozoic Appalachian orogenesis. *Geological Society of America Bulletin* **103**, 125–135.

Emeleus, C. H., (1963). Structural and petrographic observations on layered granites from southern Greenland. In: Fisher, D. J., Frueh, A. J., Hurlbut, C. S., et al. (eds) *International Mineralogical Association Papers and Proceedings of the Third General Meeting*, Washington, D.C., April 17–20, 1962. Mineralogical Society of America, Special Paper **1**, 22–29.

Fernandez, A. N. & Barbarin, B. (1991). *Enclaves and Granite Petrology*. Amsterdam: Elsevier.

Frost, T. P. & Mahood, G. A. (1987). Field, chemical and physical constraints on mafic–felsic interaction in the Lamarck Granodiorite, Sierra Nevada, California. *Geological Society of America Bulletin* **99**, 272–291.

Gilbert, G. K. (1906). Gravitational assemblage in granite. *Geological Society of America Bulletin* **17**, 321–328.

Glazner, A. F. (2014). Magmatic life at low Reynolds number. *Geology* **42**, 935–938.

Glazner, A. F., Bartley, J. M., Coleman, D. S., Gray, W. & Taylor, R. Z. (2004). Are plutons assembled over millions of years by

amalgamation from small magma chambers? *GSA Today* **14**, 4–11.

Glazner, A. F., Bartley, J. M., Law, B. & Coleman, D. S. (2012). Ladder dikes, crazy geochemistry and liquid immiscibility in otherwise sane granites. *Geological Society of America, Abstracts with Programs* **44**, 21.

Gorner, E. (2016). A mapping, petrographic, and mineral chemistry study of intrusions in the Tilting Igneous Suite, Fogo Island, Newfoundland. BSc Honors thesis, Memorial University of Newfoundland, St John's, pp. 1–69.

Hamilton, M. A. & Kerr, A. (2016). New U–Pb dates from Silurian rocks on Fogo Island: Preliminary stratigraphic and tectonic implications. *Current Research, Newfoundland and Labrador Department of Natural Resources Geological Survey* **16**, 123–132.

Kerr, A. (2013). The Fogo Process from a Geologist's Perspective: A Discussion of Models and Research Problems. *Current Research, Newfoundland and Labrador Department of Natural Resources Geological Survey* **13**, 233–265.

Leung, J. S. (1974). Sector-zoned titanaugites: Morphology, crystal chemistry, and growth. *American Mineralogist* **59**, 127–138.

Marsh, B. D. (1981). On the crystallinity, probability of occurrence, and rheology of lava and magma. *Contributions to Mineralogy and Petrology* **78**, 85–98.

Marsh, B. D. (2002). On bimodal differentiation by solidification front instability in basaltic magmas, part 1: basic mechanics. *Geochimica et Cosmochimica Acta* **66**, 2211–2229.

McNicoll, V. C., Squires, G. C., Wardle, R. J., Dunning, G. R. & O'Brien, B. H. (2006). U–Pb geochronological evidence for Devonian deformation and gold mineralization in the eastern Dunnage Zone, Newfoundland. *Current Research, Newfoundland and Labrador Department of Natural Resources Geological Survey* **06**, 45–60.

Miller, C. F., Furbish, D. J., Walker, B. A., Claiborne, L. L., Koteas, G. C., Bleick, H. A. & Miller, J. S. (2011). Growth of plutons by incremental emplacement of sheets in crystal-rich host: evidence from Miocene intrusions of the Colorado River region, Nevada, USA. *Tectonophysics* **500**, 65–77.

Miller, J. S., Matzel, J. E. P., Miller, C. F., Burgess, S. D. & Miller, R. B. (2007). Zircon growth and recycling during the assembly of large composite arc plutons. *Journal of Volcanology and Geothermal Research* **167**, 282–299.

Paterson, S. (2009). Magmatic tubes, pipes, troughs, diapirs, and plumes: Late-stage convective instabilities resulting in compositional diversity and permeable networks in crystal-rich magmas of the Tuolumne batholith, Sierra Nevada, California. *Geosphere* **5**, 496–527.

Pearce, J. A. (1982). Trace Element Characteristics of Lavas from Destructive Plate Boundaries. In: Thorpe, R. S. (ed.) *Andesites*. Chichester: John Wiley, pp. 525–548.

Petford, N., Cruden, A. R., McCaffrey, K. J. W. & Vigneresse, J. L. (2000). Granite magma formation, transport and emplacement in the Earth's crust. *Nature* **408**, 669–673.

Philpotts, A. & Carroll, M. (1996). Physical properties of partly melted tholeiitic basalt. *Geology* **24**, 1029–1032.

Pollock, J. C., Wilton, D. H. C., van Staal, C. R. & Morrissey, K. D. (2007). U–Pb detrital zircon geochronological constraints on the early Silurian collision of Ganderia and Laurentia along the Dog Bay Line: The terminal lapetan suture in the Newfoundland Appalachians. *American Journal of Science* **307**, 399–433.

Rutter, E. H. & Neumann, D. H. K. (1995). Experimental deformation of partially molten Westerly granite under fluid-absent conditions, with implications for the extraction of granitic magmas. *Journal of Geophysical Research: Solid Earth* **100**, 17697–15715.

Sandeman, H. A. & Malpas, J. (1995). Epizonal I and A-type granites and associated ash-flow tuffs, Fogo Island, northeast Newfoundland. *Canadian Journal of Earth Sciences* **32**, 1835–1844.

Schleicher, J. M., Bergantz, G. W., Breidenthal, R. E. & Burgisser, A. (2016). Time scales of mixing in magma mushes. *Geophysical Research Letters* **43**, 1543–1550.

Stern, C., Huang, W. & Wyllie, P. (1975). Basalt–andesite–rhyolite–$H_2O$: Crystallization intervals with excess $H_2O$ and $H_2O$-undersaturated liquidus surfaces to 35 kilobars, with implications for magma genesis. *Earth and Planetary Science Letters* **28**, 189–196.

Storm, S., Shane, P., Schmitt, A. K. & Lindsay, J. M. (2012). Decoupled crystallization and eruption histories of the rhyolite magmatic system at Tarawera volcano revealed by zircon ages and growth rates. *Contributions to Mineralogy and Petrology* **163**, 505–519.

Streck, M. J. (2008). Mineral textures and zoning as evidence for open system processes. In: *Mineralogical Society of America and Geochemical Society, Reviews in Mineralogy and Geochemistry* **69**, 595–622.

Taylor, S. R. & McLennan, S. M. (1985). *The Continental Crust; Its Composition and Evolution; an Examination of the Geochemical Record Preserved in Sedimentary Rocks*. Oxford: Blackwell.

Vernon, R. H. & Paterson, S. R. (2006). Mesoscopic structures resulting from crystal accumulation and melt movement in granites. *Transactions of the Royal Society of Edinburgh: Earth Sciences* **97**, 369–381.

Walker, B. A., Jr, Miller, C. F., Claiborne, L. L., Wooden, J. L. & Miller, J. S. (2007). Geology and geochronology of the Spirit Mountain batholith, southern Nevada: Implications for timescales and physical processes of batholith construction. *Journal of Volcanology and Geothermal Research* **167**, 239–262.

Webber, J. R., Klepeis, K. A., Webb, L. E., Cembrano, J., Morata, D., Mora-Klepeis, G. & Arancibia, G. (2015). Deformation and magma transport in a crystallizing plutonic complex, Coastal Batholith, central Chile. *Geosphere* **11**, 1401–1426. doi:10.1130/GES01107.1.

Weinberg, R. F., Sial, A. N. & Pessoa, R. R. (2001). Magma flow within the Tavares pluton, northeastern Brazil: compositional and thermal convection. *Geological Society of America Bulletin* **113**, 508–520.

Wiebe, R. (1968). Plagioclase stratigraphy; a record of magmatic conditions and events in a granite stock. *American Journal of Science* **266**, 690–703.

Wiebe, R. A. (1996). Mafic–silicic layered intrusions: the role of basaltic injections on magmatic processes and the evolution of silicic magma chambers. *Earth and Environmental Science Transactions of the Royal Society of Edinburgh* **87**, 233–242.

Wiebe, R. & Collins, W. (1998). Depositional features and stratigraphic sections in granitic plutons: implications for the emplacement and crystallization of granitic magma. *Journal of Structural Geology* **20**, 1273–1289.

Wiebe, R., Manon, M., Hawkins, D. & McDonough, W. (2004). Late stage mafic injection and thermal rejuvenation of the Vinalhaven granite, coastal Maine. *Journal of Petrology* **45**, 2133–2153.

Wiebe, R., Jellinek, M., Markley, M., Hawkins, D. & Snyder, D. (2007). Steep schlieren and associated enclaves in the Vinalhaven granite, Maine: possible indicators for granite rheology. *Contributions to Mineralogy and Petrology* **153**, 121–138.

Williams, H. (1993). Acadian orogeny in Newfoundland. In: Roy, D. C. and Skehan, J. W. (eds) The Acadian Orogeny: Recent Studies in New England, Maritime Canada and the Autochthonous Foreland. *Geological Society of America, Special Papers* **275**, 123–133.

Yücel, C., Arslan, M., Temizel, İ. & Abdioğlu, E. (2014). Volcanic facies and mineral chemistry of Tertiary volcanics in the northern part of the Eastern Pontides, northeast Turkey: implications for pre-eruptive crystallization conditions and magma chamber processes. *Mineralogy and Petrology* **108**, 439–467.

Zavala, K., Leitch, A. M. & Fisher, G. (2011). Silicic segregations of the Ferrar Dolerite Sills. *Journal of Petrology* **52**, 1927–1964.